Journal of Inclusion Phenomena and Macrocyclic Chemistry (2022) 102:451–476
https://doi.org/10.1007/s10847-022-01138-1

REVIEW ARTICLE

Review on fluorescent sensors-based environmentally related toxic mercury ion detection

Duraisamy Udhayakumari[1]

Received: 21 September 2021 / Accepted: 9 March 2022 / Published online: 29 April 2022

Abstract

Mercury is a frequent, bioaccumulative, extremely toxic pollutant in the environment. Mercury contamination can be accumulated along the food chain and cause a wide range of serious threats to living organisms, and also affect neurological systems and the kidneys. The trace-level detection of heavy and toxic metal ions such as mercury ions is certainly great intense. Chromogenic and fluorogenic recognition of toxic mercury ions has been established to be powerful methods due to their high detection limit, cost-efficiency, simplicity, and applicability in bioimaging. This review will mainly focus on the sensing mechanisms of fluorescent probes that have emerged over the past 5 years, such as PET, ICT, AIE, as well as ring-opening sensing mechanisms.

Keywords Mercury ions · Toxicity · Fluorescence · Mechanism · Detection limit · Bioimaging

Introduction

Fluorescent chemosensors capable of selectively recognizing heavy and toxic ions are an important target in the field of supramolecular chemistry due to their potential application in bioimaging molecular catalysis, environmental detection, medicine, industrial processes, and human sciences [1–3]. Mercury is a toxic environmental pollutant. Due to the extreme toxicity of mercury ions, the World Health Organization (WHO) has determined that the allowable limit of mercury ions in drinking water is 0.5 µg/l [4]. There are many different techniques used to detect the concentration of toxic anions and cations present in water. These methods can be divided into four categories: mechanical, optical, electrochemical, and spectroscopic/spectrometric. Usually, the methods of high-performance liquid chromatography (HPLC), mass spectrometry, atomic emission spectroscopy (AES), atomic absorption spectroscopy (AAS), chromatography, inductively coupled plasma mass spectroscopy (ICP-MS), flow injection analysis, and electrochemical methods are used to analyze the toxic ions [5]. However, these methods suffer either from extensive, time-consuming procedures, or the use of sophisticated instrumentation. The instrumentation methods are not very expedient and versatile for ion detection. The development of chromogenic sensors is increasingly appreciated since naked eye detection can offer qualitative and quantitative information without resorting to any spectroscopic instrumentation. Fluorescence measurement, on the other hand, is usually very sensitive, versatile, and offers a sub-micromolar estimation of guest species [6, 7]. The photo-induced electron transfer, intramolecular charge transfer, ring-opening, and chelation-enhanced fluorescence mechanisms are commonly adopted fluorescence response mechanisms for mercury detection [8, 9]. A few reviews only described the mercury fluorescence sensors from different perspectives, such as molecule types, application in imaging, testing of mercury, and optical and fluorescence recognition [10–12]. This review mainly focuses on the fluorescent recognition mechanisms for the detection of mercury ions since 2015. The review is instigated with a brief discussion of the metal's occurrence, methodologies for detection, sources, applications, toxicity, and the mechanism of the mercury ion sensor. Further, the fluorogenic and chromogenic mercury ion sensors are classified according to their sensing mechanisms (Table 1).

✉ Duraisamy Udhayakumari
udhaya.nit89@gmail.com

[1] Department of Chemistry, Rajalakshmi Engineering College, Chennai 602105, India

Table 1 Summary of mercury detection using colorimetric and fluorescent chemosensor method

Sensor no.	Functional group	Sensing ions	Solvent medium	Mechanism	LOD	Applications	Reference no.
S1	Naphthalimide-sulfamethizole	Hg^{2+}	DMSO-water	AIEE	14.7 nM	Environmental water samples	20
S2a–b	Sulfonamidospirobifluorenes	Hg^{2+} and glutathione	DMSO-water	AIEE	10.4 & 103.8 nM	Environmental water samples	21
S3	Benzylidene	Hg^{2+} & CN^{-}	DMF-water	AIEE	6.6 nM	–	22
S4	Tetraphenylethene	Hg^{2+}	CH_3CN-H_2O	AIEE	–	Bioimaging studies	23
S5	Gold(I) Complex	Hg^{2+}	CH_3CN-H_2O	AIEE	–	–	24
S6	Hydroxyquinoline	Hg^{2+} & CN^{-}	DMF—H_2O	AIEE	0.24 nM	Test kit studies	25
S7	Cyanostilbene	Hg^{2+}	THF-H_2O	AIEE	37 nM	Environmental water samples	26
S8	Dimethylquinolin	Hg^{2+} & I^{-}	DMSO-water	AIEE	71.8 nM	Real water and urine samples	27
S9	Tetraphenylethene	Hg^{2+}	THF-H_2O	AIEE	10 µM	Environmental water samples	28
S10	Tetraarylethylene	Hg^{2+}	CH_3CN-H_2O	AIEE	48 nM	–	29
S11	Nanoparticles	Hg^{2+}	THF-H_2O	AIEE	22.7 nM	Bioimaging studies	30
S12	Pyridopyrazine	Hg^{2+}	CH_3CN-H_2O	AIEE	11.4 µM	Test kit studies	31
S13a–b	Schiff bases	Hg^{2+}	THF-H_2O	AIEE	19.4 & 9.84 nM	Bioimaging studies	32
S14	Cephalexin	Hg^{2+}	H_2O	AIEE	–	–	33
S15a–b	Cyanostilbene	Hg^{2+}	DMSO-water	AIEE	0.11 µM	–	34
S16	Cyanostilbene	Hg^{2+}	THF-H_2O	AIEE	3.4 nM	Bioimaging studies	35
S17	Anthracene	Hg^{2+}	THF-H_2O	AIEE	3.6 µM	Bioimaging studies	36
S18	Pyrene	Hg^{2+}	Ethanol/PBS	ICT	1.49 nM	Bioimaging studies	38
S19	Acenaphtoquinoxaline	Hg^{2+}	CH_3CN-H_2O	ICT	42 µM	–	39
S20	Benzopyran	Hg^{2+}	CH_3CN-H_2O	ICT	0.14 µM	Bioimaging studies	40
S21	Bithiophene	Hg^{2+}	Ethanol- H_2O	ICT	19 nM	Water, seafood, urine and live cells	41
S22	Coumarin	Hg^{2+}	HEPES buffer – DMSO	ICT	2.7 nM	Environmental water samples	42
S23	Phenothiazine	Hg^{2+}	Ethanol- H_2O	ICT	0.12 nM	Test strips & Bioimaging studies	43
S24	Oligothiophene	Hg^{2+}	Ethanol- H_2O	ICT	62 nM	Test strips & Bioimaging studies	44
S25	Piperazine	Hg^{2+}	DMSO-water	PET	19.2 nM	Bioimaging studies	46
S26	BODIPY	Hg^{2+}	CH_3CN-H_2O	PET	18 µM	Logic gate	47
S27	Calix[6]arene	Hg^{2+}	THF-H_2O	PET	–	–	48
S28	Fluorescein	Hg^{2+}	Methanol-Buffer	PET	22 µM	Bioimaging studies	49
S29	Imine	Hg^{2+}	Methanol/water	PET	0.28 µM	Environmental water samples	50
S30	Naphthalimide	Hg^{2+}	Ethanol- H_2O	PET	0.73 nM	–	51
S31	Naphthalimide	Hg^{2+}	HEPES buffer	PET	20.66 µM	Bioimaging studies	52

Table 1 (continued)

Sensor no.	Functional group	Sensing ions	Solvent medium	Mechanism	LOD	Applications	Reference no.
S32	Thiophene	Hg^{2+}	CH_3CN-H_2O	PET	3.9 µM	Bioimaging studies	53
S33	Schiff base	Hg^{2+}	CH_3CN-H_2O	PET	1.26 nM	Test strips	54
S34	Pyrenylthioureayl alanine	Hg^{2+}	CH_3CN: DCM	PET	93 nM	–	55
S35	Quantum dots	Hg^{2+}	Water	PET	1 pM	Environmental water samples	56
S36	Metal–organic framework	Hg^{2+}	Water	PET	17.6 nM	–	57
S37	Polyaniline nanoclips	Hg^{2+}	Water	PET	4 nM	Environmental water samples	58
S38	Rhodamine	Hg^{2+}	Water	PET	355 nM	–	59
S39	Rhodamine		Triethylamine	Ring opening	–	Bioimaging studies	60
S40	Rhodamine	Hg^{2+}	DMF-H_2O	Ring opening	–	Bioimaging studies	61
S41	Rhodamine	Hg^{2+}	Ethanol- H_2O	Ring opening	0.63 µM	Environmental water samples	62
S42	Rhodamine	Hg^{2+}	Ethanol- H_2O	Ring opening	1.3 µM	Bioimaging studies	63
S43a-c	Rhodamine	Hg^{2+}	Tris—HCl/ C_2H_5OH	Ring opening	18 nM, 16 nM, 56 nM	Bioimaging studies	64
S44	Rhodamine	Hg^{2+}	CH_3CN-H_2O	Ring opening	0.53 µM	–	65
S45	Rhodamine	Hg^{2+}	HEPES buffer/ methanol	Ring opening	1.5 nM	Skin-lightening cream	66
S46	Rhodamine	Hg^{2+}	THF-H_2O	Ring opening	27 µM	–	67
S47	Rhodamine	Hg^{2+}	HEPES buffer-CH_3CN	Ring opening	0.49 µM	Test strips	68
S48	*p*-tert-Butylcalix[4]arene	Hg^{2+}	Ethanol–water	Ring opening	9.6 nM	Bioimaging studies	69
S49	Rhodamine	Hg^{2+}	CH_3CN-HEPES buffer	Ring opening	0.14 µM	Bioimaging studies	70
S50	Rhodamine	Hg^{2+}	CH_3CN	Ring opening	0.2 µM	–	71

Metal occurrence

Mercury is a naturally occurring element found in rock in the earth's crust. It is released into the environment from volcanic activity, forest fires, and weathering of rocks. Mercury exists in several forms, such as metallic mercury, inorganic mercury, methyl mercury, and other organic mercury compounds [13]. Elemental mercury is a silver-white metal and is liquid at room temperature. The inorganic mercury compounds are obtained when other elements (S, O, Cl, etc.,) combine with mercury. Methylmercury is the most common organic mercury compound found in the environment. The inorganic mercury is converted to the organic form when the microscopic organisms unite mercury with carbon (Fig. 1).

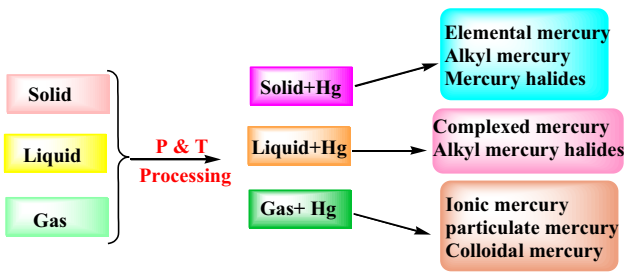

Fig. 1 Distribution of mercury in the environment

Sources, applications, and toxic effect of mercury

Sources

Among the metal ions, particular attention has been paid to mercury ions for their extreme toxicity. Mercury contamination occurs through various natural processes such as volcanic eruptions, geothermal springs, geologic deposits, and emissions from the ocean. Human activity is the main cause of mercury releases, particularly coal-fired power stations, burning oil, fossil fuels, raw materials, residential coal burning for heating and cooking, industrial processes, waste incinerators, and as a result of mining for mercury, gold, and other metals. Some of the mercury circulating through today's environment was released years ago. Water, land, and other surfaces can repeatedly re-emit mercury to the atmosphere after its initial release into the environment [14]. The anthropogenic emissions continue to add significantly to the global pool of mercury (Fig. 2).

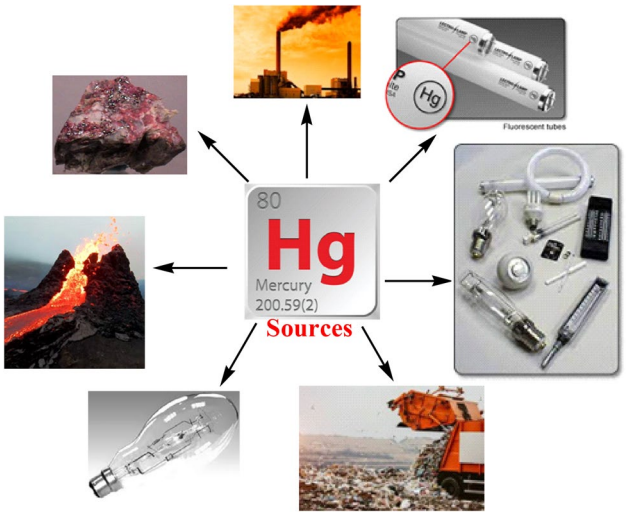

Fig. 2 Sources of mercury

Applications

Mercury is used in various processes and workplaces. Mercury is used in laboratories for making thermometers, barometers, diffusion pumps, fluorescent lamps, electrical apparatus and instruments, mercury switches, mercury relays, sphygmomanometers, and used as an electrode for making batteries. Mercury is also used as a catalyst in chemical industries. Mercury easily forms alloys with other metals such as gold, silver, and tin, called amalgams. Mercury amalgams were also used in dental fillings. Metal mercury is used as a liquid electrode in the manufacture of chlorine and sodium hydroxide by electrolysis of brine [15]. Mercurous chloride (Hg_2Cl_2) is used in medicine as a purgative and also used as a standard electrode in electrochemical measurements (Fig. 3).

Major consequences and adverse effects of mercury

Mercury (Hg^{2+}) is well known as one of the most toxic metals, and is widespread in air, water, and soil, generated by many sources such as gold production, coal plants, thermometers, barometers, caustic soda, and mercury lamps. As it can cause strong damage to the central nervous system, the accumulation of mercury in the human body can lead to various cognitive and motor disorders, and Minamata disease. A major absorption source is related to daily diet such as fish. Thermometer manufacturing releases a very small amount of mercury (from 0.1 mg to 10 mg) into the atmosphere, which contaminates the soil. This can cause harmful effects, such as nerve, brain, and kidney damage, lung irritation, eye irritation, skin rashes, vomiting, and diarrhea. Metallic mercury mainly causes health effects including neuromuscular changes, headaches, changes in nerve responses, tremors, insomnia, etc. [16] when inhaled as a vapor where it can be absorbed through the lungs (Fig. 4).

Marine organisms like phytoplankton and zoo-planktons easily absorb the toxic methylmercury compound. The organisms are consumed by small fish, which are consumed

Fig. 3 Applications of mercury

Fig. 4 Impacts of mercury

by large fish, and the large fish are consumed by human beings [17]. The poisonous chemical enters the body of human beings through the food chain. It causes various disorders such as nervous disorders, muscular coordination, severe headaches, and loss of vision and hearing (Fig. 5).

Methodologies for mercury ion detection

In recent years, various accurate and analytical techniques have been reported for the detection of mercury ions such as gas chromatography-triple quadrupole mass spectrometry (GC–MS/MS), mercury analyzers, electrochemical sensors, cold vapor integrated quartz crystal microbalance (CV-QCM), atomic absorption spectroscopy, atomic fluorescence spectroscopy, reduced graphene oxide field-effect transistor (rGO FET), solid-phase extraction, and fluorescence and colorimetric methods. Different types of nanozymes are used to detect mercury ions due to their simplicity and ease of developing a portable sensor. The processing of hydrocarbon samples is generally very complex, and mercury is found in low concentrations. Therefore, the development of highly sensitive analytical methods is still needed for low-level detection of mercury ions. The colorimetry and fluorescent methods are widely used because these methods have an excellent selectivity compared to other methods [18].

Mechanism of mercury sensing

Fluorescence emission takes place from the electronically excited states of molecules. However, given the high reactivity of the electrons in these states, reactions that usually do not occur in the ground states can take place. From the point of view of chemical sensing, the coordination of metal ions could cause an enhancement of the fluorescence or quenching of the fluorescence intensity. The enhancement of fluorescence emission is called the chelation enhanced fluorescence effect (CHEF). The quenching of the fluorescence is called the chelation enhancement quenching effect (CHEQ). Both effects can be coupled with a red or blue shift of the emission band. Upon analyte binding to chemosensors, it is possible to modulate some of these reactions' emissions, and thus take advantage of the different mechanisms for signal transduction (Fig. 6). Conventional mechanisms such as

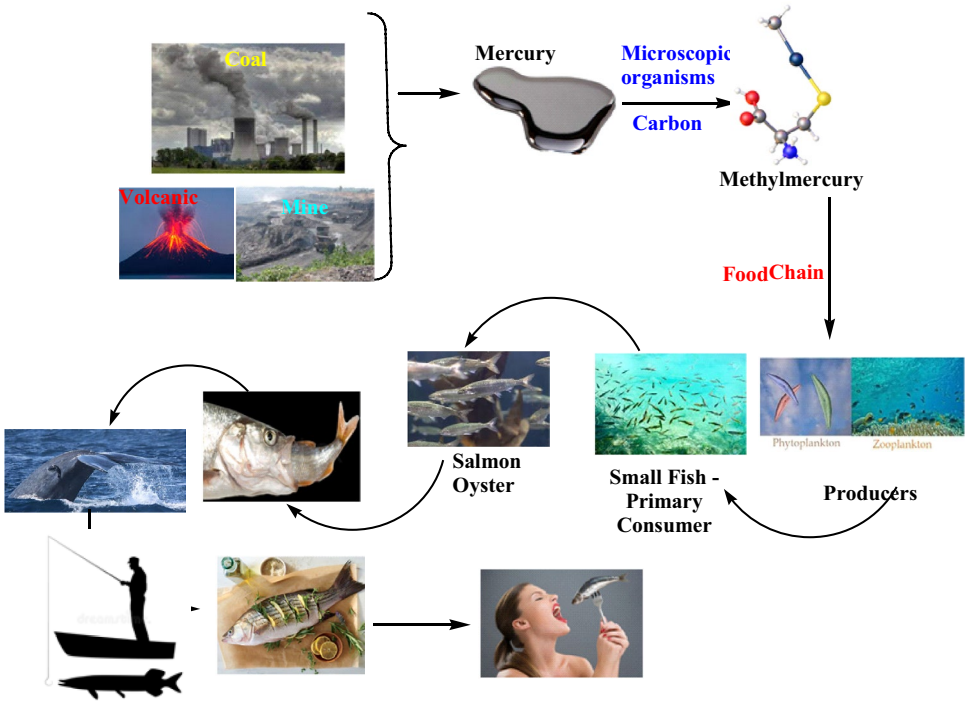

Fig. 5 Bioaccumulation of mercury

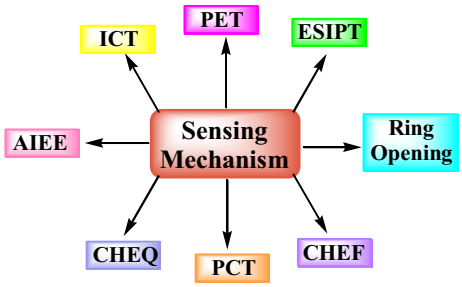

Fig. 6 Various fluorescence sensing mechanism

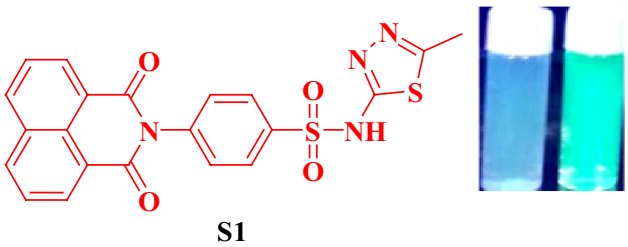

S1

Fig. 8 Structure of **S1**

paramagnetic fluorescence quenching, photo-induced electron transfer (PET), intramolecular charge transfer (ICT), fluorescence resonance energy transfer (FRET), photo-induced charge transfer (PCT), photo-induced excimer formation, intersystem crossing or the heavy atom effect, aggregation-induced emission (AIE) and excited-state intramolecular proton transfer (ESIPT) have been frequently adopted for the construction of probe molecules.

Fluorescent sensors for mercury ions

Aggregation-induced emission (AIE)-based Hg^{2+} ions detection

The restriction of intramolecular motion, rotation, or vibration (RIM, RIR, or RIV) in the aggregates is the main cause of the AIE phenomenon. The AIE active molecules are weakly emissive in the solution state due to unhindered intramolecular motions but become highly emissive upon aggregation in a suitable environment through activation of RIM, RIR, or RIV mechanisms in the excited state. In view of such unusual fluorescence behaviors, the AIE phenomenon is successfully utilized to design fluorescent probes with proper chelating groups for the detection of metal ions [19]. The aggregation of AIE probes can be tuned by metal ions through electrostatic interaction, coordination interaction, or the influence of polarity and viscosity (Fig. 7).

Highly fluorescent aggregation-induced emission-based 1, 8-naphthalimide-sulfamethizole sensor **S1** has been

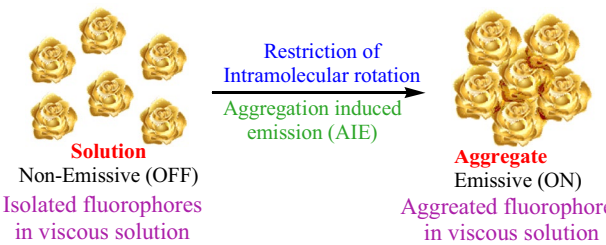

Fig. 7 Aggregation-induced emission

reported for Hg^{2+} and Ag^{+} ions. Aggregation-induced emission is caused by the hydrophobic nature of naphthalimide fluorogenic moiety in DMSO: water (1:99 v/v, pH 7.2, HEPES buffer). Upon the addition of various metal ions, Hg^{2+} ions show an increase in absorbance at 267 and 343 nm with a slight red shift (hypochromic effect). An excimer group was obtained from the intramolecular interaction between the naphthalimide moieties in the completion of **S1** with Hg^{2+} ion [20]. Due to this reason, Sensor **S1** emission band at 390 nm was quenched and a new intensity band appeared at 483 nm in the presence of Hg^{2+} ions. The sensor **S1**-Hg^{2+} coordination restricts the free rotations of the **S1** and increases the rigidity of the molecular assembly, resulting in enhanced fluorescence intensity at 483 nm. Further, significantly enhancing fluorescence intensity was observed by the increasing addition of Hg^{2+} ions. Mercury ions induce more aggregation of the **S1**-Hg^{2+} complex thereby facilitating the aggregation-induced emission enhancement behavior of the **S1**. Sensor **S1** sensitively detects Hg^{2+} ions and the calculated detection limit of **S1**-Hg^{2+} ions is 14.7 nM (Fig. 8).

A new fluorescent sensor **S2a–b** based on sulfonamidospirobifluorenes was synthesized and reported for the selective detection of Hg^{2+} ions in the DMSO/HEPES buffer mixture [21]. Out of 20 metal ions, sensor **S2a–b** only shows an excellent selectivity towards Hg^{2+} ions and showed a selective fluorescence quenching (107-fold). The sulfonamide group coordinates to Hg^{2+} ions that direct to an aggregation of such complex via the face-to-face stacking of the spirobifluorene cores. At neutral pH, the sulfonamide group coordinates with Hg^{2+} ions and could promote deprotonation of the –NH group in **S2a–b**. The detection limits of **S2a–b** with Hg^{2+} ions were found to be 10.4 nM and 103.8 nM for the derivatives bearing two and four sulfonamide groups, respectively (Fig. 9).

Li et al. reported [22] a novel fluorescence sensor **S3** for selective and sensitive detection for Hg^{2+} and CN^{-} ions in DMF-H_2O (13:12, v/v). Sensor **S3** shows a nonemissive spectrum in a pure organic solvent (DMF) and low concentrated aqueous system. When the water content is increased to 60%, the fluorescence emission band at 650 nm increased significantly, and in 80% water the emission intensity band

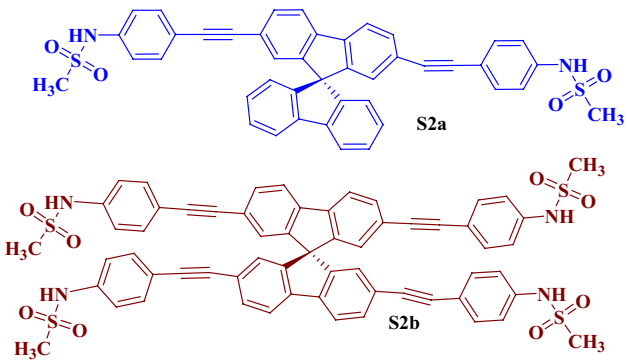

Fig. 9 Structure of **S2a–b**

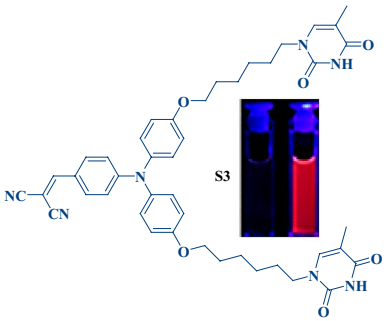

Fig. 10 Structure of **S3**

reached its maximum (120 fold). A slight decrease in fluorescence intensity was observed when adding further water in **S3**. This is due to the formation of amorphous aggregates. The emission intensity of **S3** gradually inclined and reaches the maximum along with a small bathochromic shift (50 nm) upon the addition of Hg^{2+} ions. Under a UV lamp (360 nm), the **S3**-Hg^{2+} complex results in a strong red fluorescence, and the calculated detection limit to be 6.6 nM. The enhancement of fluorescence is due to the aggregation induced by the coordination of thymine units with Hg^{2+} ions (Fig. 10).

A novel aggregation-induced emission-based sensor **S4** designed [23], synthesized, and reported for selective recognition of Hg^{2+} ions in a mixture of CH_3CN: H_2O (60%). Sensor **S4** was further used to quantitatively measure the bioaccumulation of Hg^{2+} within a small invertebrate, *D. carinata* (Fig. 11). When exciting sensor **S4** at 350 nm, the emission intensity increased from 0.17 to 1038.6 upon the gradual addition of Hg^{2+} ions (6100-fold). *D. carinata* alone shows no fluorescence signals and when incubated in **S4** showed blue fluorescence (460–500 nm). In the presence of Hg^{2+} ions, *D. carinata*-**S4** showed red fluorescence in the red channel in the 570 to 610-nm wavelength range. The fluorescent microscopy studies recognize in vivo dispersion and distribution of Hg^{2+} in *D. carinata*.

X. Han and research group [24] designed a gold (I) complex sensor **S5** and reported for Hg^{2+} ion detection in CH_3CN-H_2O (1 : 1, V : V) solution. Usually, gold (I) complexes show unique optical properties because of their intermolecular gold–gold interactions. Sensor **S5** reveals an aggregate-induced emission (AIE) in CH_3CN-H_2O mixtures and exhibits a high selectivity towards Hg^{2+} ions. In a pure CH_3CN sensor, **S5** exhibits almost no emission. When increasing the percentage of water (60%) in sensor **S5**, CH_3CN: H_2O, 40:60) results in a fluorescence enhancement band at 572 nm with a hypochromatic shift to 536 nm. The increasing percentage of water endorses the aggregation of sensor **S5** and changes its form from a well-dispersed state to an aggregated state, which induces the emission (Fig. 12). The addition of Hg^{2+} ions into **S5** exhibited an effective fluorescence quenching over the other metal ions such as Al^{3+}, Ca^{2+}, Cd^{2+}, Cu^{2+}, Fe^{2+}, K^+, Li^+, Mn^{2+}, Na^+, Ni^{2+}, Pb^{2+}, Ag^+, Zn^{2+}, and Fe3$^+$ ions. Exciting **S5** at 340 nm exhibited a strong fluorescence emission at 575 nm in the presence of Hg^{2+} ions.

A novel 8-hydroxyquinoline functionalized pillar[5]arene sensor **S6** was synthesized and the sensor selectively recognizes toxic Hg^{2+} ions based on the AIE fluorescence mechanism in an aqueous solution [25]. Sensor **S6** almost shows non-fluorescence in a pure organic system (DMF). On increasing the water content, **S6** displays strong fluorescence emission intensity at 410 nm (7.88-fold) due to aggregation of fluorescence. Upon the addition of various metal ions into **S6**, Hg^{2+} ions could significantly quench the fluorescence over other ions at 410 nm. Under a UV lamp,

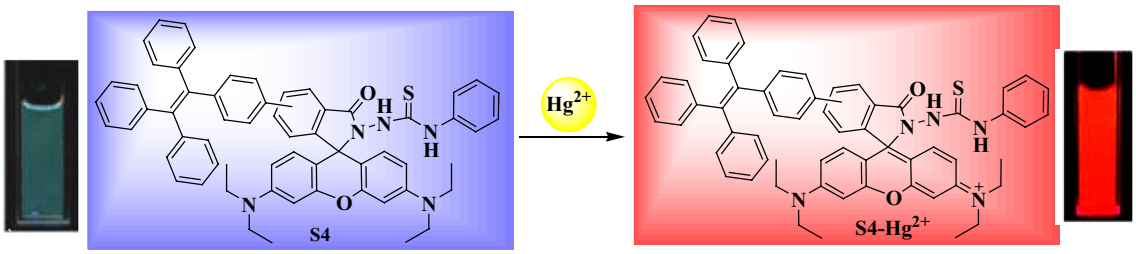

Fig. 11 Structure of **S4**

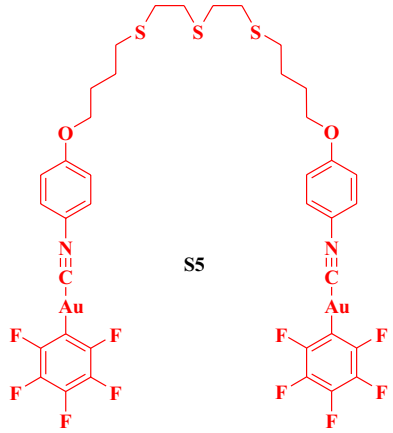

Fig. 12 Structure of **S5**

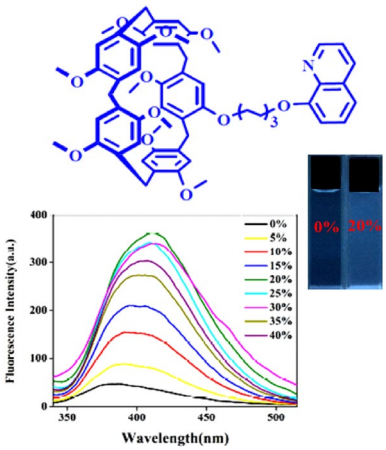

Fig. 13 Structure of **S6**

the fluorescence color of **S6** (20% H_2O) changed from blue to colorless upon the addition of Hg^{2+} ions (Fig. 13). The detection limit of **S6** towards Hg^{2+} ions was calculated to be 0.24 nM. Further, based on the above results, the Hg^{2+} detection test kit was prepared by using an **S6** sensor on a silica gel plate and the test kit could detect Hg^{2+} ions more conveniently and effectively.

Cyanostilbene derivative fluorescent sensor **S7** was developed for selective and sensitive detection of Hg^{2+} ions in THF/H_2O (2:8, v/v) medium [26]. Sensor **S7** shows three absorption bands at 245, 291, and 365 nm. Sensor **S7** has a longer π-conjugated unit and showed a blue-shift band due to a more twisted conformation caused by the cyano and vinyl groups (Fig. 14). When **S7** dispersed in its "solution" state (THF), sensor **S7** showed a non-emissive property. Upon the addition of water (80%), THF had a rigorous band at 537 nm and the fluorescence intensity enhanced by 79 times compared to the emission spectrum in pure THF and THF with a small fraction of water. These results correlated well

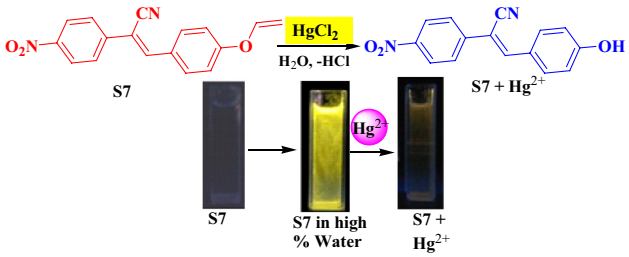

Fig. 14 Structure of **S7**

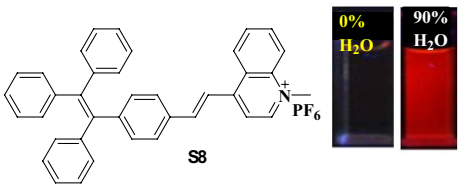

Fig. 15 Structure of **S8**

with the fact that more aggregates were formed in lesser solvents. The enhanced fluorescence of **S7** (THF-H_2O) can be quenched linearly upon interacting with Hg^{2+} ions. The detection limit of Hg^{2+} is 37 nM.

Sensor **S8** was prepared by condensation of 1,4- dimethylquinolin-1-ium iodide with 4-(1,2,2-triphenylvinyl) benzaldehyde under a refluxed condition in ethanol [27]. Highly fluorescent sensor **S8** was further applied for the detection of Hg^{2+} ions in an aqueous medium. Sensor **S8** is based on a tetraphenylethene functionalized quinolinium salts with hexafluorophosphate (PF_6^-) as the counterion and exhibits non-fluorescence properties in pure DMSO solution. When increasing the water fraction from 0 to 80% into **S8**, it exhibits a very low-level emission intensity spectrum. Above 80% of water in DMSO, the emission band at 610 nm enhanced sharply, and reaches a maximum (13-fold) when compared to pure DMSO solution. Meanwhile, the colorless sensor **S8** solution is converted into strong red emission color under the UV light at 365 nm (Fig. 15). The observed fluorescence changes could be recognized as the formation of molecular aggregates, which suppresses the non-radiative relaxation channels. Upon the addition of I^- fluorescence, emission of **S8** started quenching. The quenching of fluorescence is due to synergetic electrostatic interaction and drastic collision between aggregates of **S8** and I^-. Fluorescence "Turn-On" was observed when **S8**- I^- complex interact with Hg^{2+} ions and the detection limit for Hg^{2+} is as low as 71.8 nM.

Fluorescence sensor **S9** has been prepared by reaction of tetraphenylethene containing ketone with 1, 2-ethanedithiol [28] and reported for detection of Hg^{2+} ions THF/H_2O mixtures. In THF solution state sensor **S9** shows a nearly nonemissive property. Upon the addition of water, the aggregates

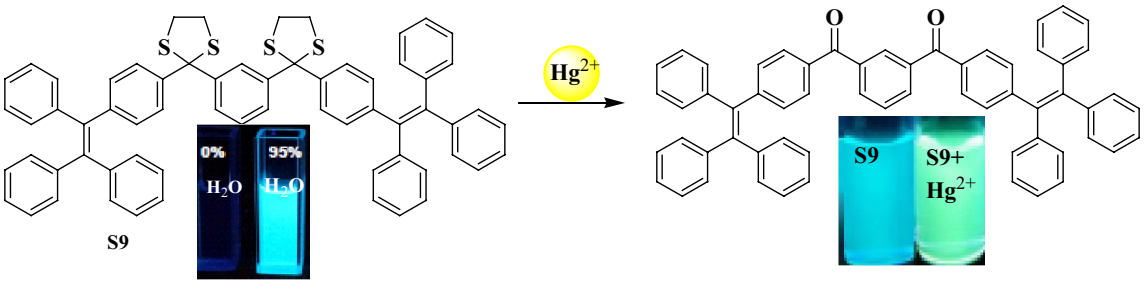

Fig. 16 Sensing mechanism of **S9** with Hg^{2+} ions

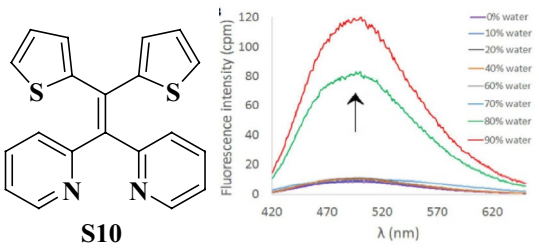

Fig. 17 Structure of **S10**

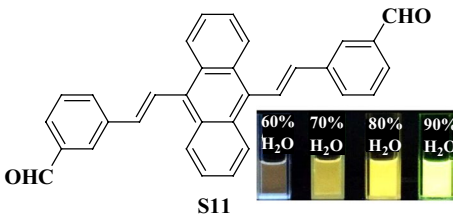

Fig. 18 Structure of **S11**

of sensor **S9**AIEgens were formed and the fluorescence emission intensity of AIEgens increased promptly when a large amount of water was added (> 80%) into sensor **S9**. Sensor **S9** emitted sky blue luminescence due to the breaking of the conjugated system and the changing of the intramolecular charge transfer (ICT) efficiency upon excitation at the aggregation state. Upon the addition of Hg2 + ions, the absorption peak at 316 nm redshifted to 338 nm. When introducing mercury ions into **S9**, the luminescent color change from sky blue to yellow-green could happen instantly over the other metal ions. The detection limit of **S9** towards Hg^{2+} ions was calculated to be 10 µM (Fig. 16).

Tetraarylethylenes with metal chelating 1,1-bis(2-pyridylethylene) fragments and thiophene/bithiophene substituents-based sensor **S10** have been prepared by Gabr and Pigge [29]. Sensor **S10** acts as an AIE active fluorescent sensor for Hg^{2+} ions detection. In a pure CH_3CN sensor, **S10** revealed a weak fluorescence emission at 512 nm. The addition of H_2O into **S10** initially shows a slight red-shifted emission band followed by a decrease in emission intensity at 520 nm and the appearance of a new blue-shifted emission band at 404 nm. Further increasing the water fraction in **S10** (9:1 H_2O: CH_3CN), the enhanced emission intensity band was observed at 404 nm. The sensors exhibit red-shifted and enhanced emission in the presence of Hg^{2+} in an aqueous solution. The limit of detection for Hg^{2+} was determined to be 48 nM (Fig. 17).

A dual-emission ratiometric fluorescent sensor **S11** based on AIE organic fluorescence nanoparticles and Au nanoclusters for detection of Hg^{2+} ion has been reported by Niu and coworkers [30]. When sensor **S11** is in organic medium (THF), the twisted conformation makes it easy to rotate and vibrate, and the enhanced non-radiative transitions decrease its fluorescence emission intensities. Further increasing the concentration of H_2O (80%), the intramolecular rotations are restricted to some extent, so its fluorescence intensities are stronger. In 90% of H_2O, the face-to-face interactions, nonradiative transitions, and intramolecular rotation are all circumventing, thus its enhanced fluorescence emission intensity (blue shift). With increasing the concentrations of Hg^{2+} ions, the sensor displays continuous color changing from red to yellow to green and exhibits significant fluorescence quenching (Fig. 18).

A series of novel pyridopyrazine derivatives-based sensor **S12a–d** were synthesized and developed for selective and sensitive detection for Hg^{2+} ions in the H_2O-CH_3CN mixture [31]. Sensor **S12a** showed highly twisted conformation with no π-π stacking interactions. All the sensors **S12a–d** showed a weak fluorescence emission in CH_3CN solution. In higher water fractions, **S12a–b** displayed a strong enhancement of emission intensity with a slight red shift in emission maxima. Pyridopyrazine derivatives of sensors **S12a–b** bearing electron-withdrawing biphenyl rings showed "turn-on", whereas **S12c–d** bearing electron-donating biphenyl rings showed "turn-off" fluorescent response towards Hg^{2+} ions in aqueous media (Fig. 19). The detection limits of probes **S12a–d** towards Hg^{2+} were found to be in the submicromolar range. The other competitive metal ions such as Na^+, K^+, Mg^{2+}, Ca^{2+}, Ba^{2+}, Cr^{3+}, Fe^{3+}, Fe^{2+}, Co^{2+}, Ni^{2+}, Cu^{2+},

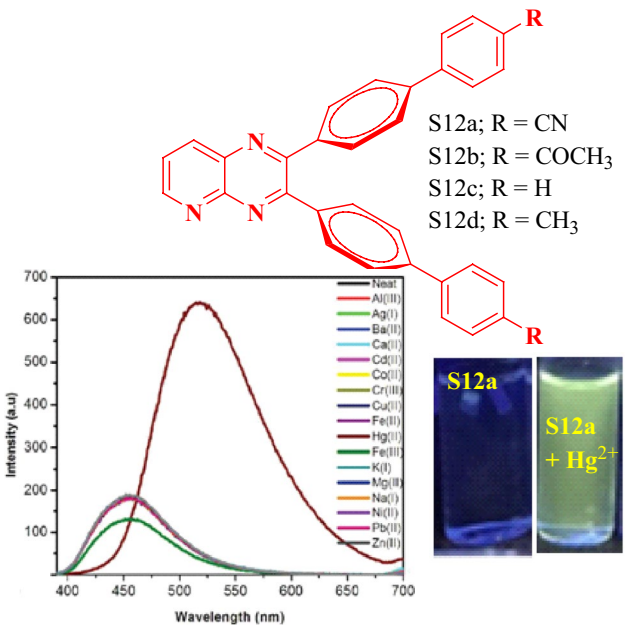

Fig. 19 Structure of **S12a–d**

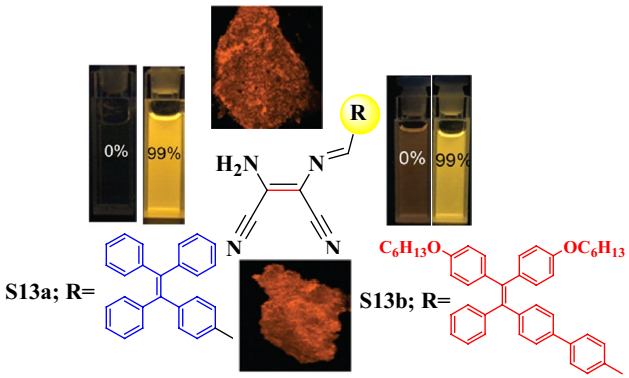

Fig. 20 Structure of **S13a–b**

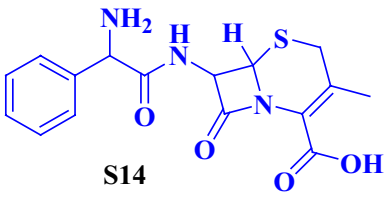

Fig. 21 Structure of **S14**

Ag^{+}, Zn^{2+}, Cd^{2+}, Al^{3+} and Pb^{2+} did not show a fluorescence response with sensors **S12a–d**.

Schiff base type-two novel fluorogenic sensors **S13a–b** containing AIE luminogen have been reported for Hg^{2+} ions in aqueous media [32]. In pure THF solution, sensor **S13a** showed almost non-fluorescence properties and **S13b** displayed weak emission intensity. When the water fraction increased from 0 to 50%, both sensors displayed a bathochromic shift. Upon the addition of excessive water (99%), the fluorescence intensity of **S13a–b** increased dramatically due to its aggregated nature. Upon increasing the concentration of water, sensors **S13a–b** could aggregate to form nanoparticles and be dispersed in water because they possessed many hydrophobic aromatic rings. Due to the two strong electron-donating alkoxy groups and longer conjugation lengths, the quantum yield of **S13b** was higher than that of **S13a** because of the stronger internal charge transfer effect. Once encountered the Hg^{2+} ions, the maximum fluorescence emission intensity of **S13a–b** gradually decreased significantly (Fig. 20).

Cephalexin molecular assembly-based fluorescence sensor **S14** prepared by Pradeep Kumar Singh et al. and reported for Hg^{2+} ion sensor [33]. An emission study shows that cephalexin has very feeble fluorescence properties while after laser treatment, a strong blue-colored fluorescence due to self-assembly fluorescence. The fluorescent assembly is shown to detect very low concentrations of Hg^{2+} ions in an aqueous solution due to the presence of a negative sulfur molecule binding site. Upon UV irradiation, the weak interaction between α-cyclodextrin and *cis*-azobenzene may drive some of the α-Cyclodextrin to slide onto the alkyl chain, and thus the self-organization of azo complexes with α-cyclodextrin could form different self-assembled aggregates. Sensor **S14** was applied for Hg^{2+} ions detection in an aqueous medium due to its affinity toward negative sulphur molecular binding site in sensor and shows fluorescence quenching (Fig. 21).

Rod-coil cyanostilbene amphiphile sensor **S15** was prepared by the Knoevenagel condensation method and reported for Hg^{2+} ions detection in an aqueous medium [34]. Applying two trifluoromethyl groups on the rod segment of **S15** is predictable to increase its hydrophobicity, which shows a strong tendency to form supramolecular assemblies with prominent aggregation-induced emission behaviors. Under UV light irradiation (365 nm), a typical orange emission signal can be directly visualized for **S15a** towards Hg^{2+}, which is distinct from green emission signals for other metal ion species. The sensor system **S15** shows an excellent selectivity toward Hg^{2+} ions over other metal ions. The detection limit for the sensor **S15** towards Hg^{2+} ions is determined to be 0.11 μM (Fig. 22).

Aggregation-induced emission (AIE) active linear conjugated Schiff base and containing α-cyanostilbene unit sensor **S16** was reported for Hg^{2+} ions detection [35]. In THF solvent, sensor **S16** was well dispersed and displayed structured absorption spectra and almost non-fluorescence emission. In the aggregation state, the twisted conformation with larger torsion angles between the benzene rings avoiding strong

Fig. 22 Structure of **S15**

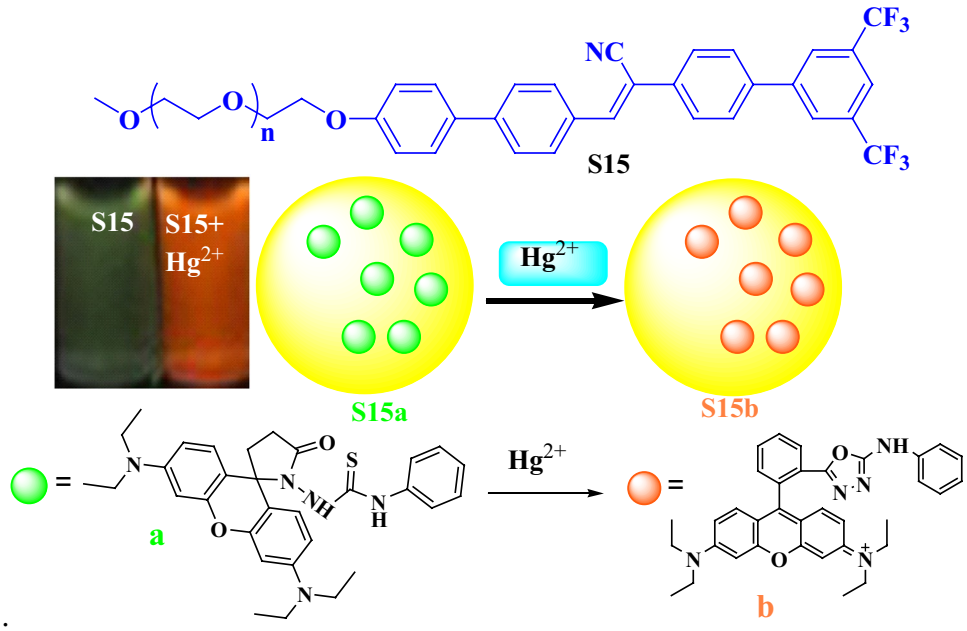

π-π stacking interactions as well as their excimer formation When increasing the percentage of water the absorbance gradually decreased and the maximal absorption wavelength blue-shifted slightly from 390 to 375 nm and an absorption peak appeared at 302 nm. These spectral changes are due to aggregating in the sensor phase by gradually increasing the water fraction. Up to 30% of the water sensor exhibits its weak fluorescence intensity and the fluorescence intensity was gradually enhanced and reached its maximum at 40% of water fraction. When increasing the percentage of water fraction, the fluorescence emission intensity gradually decreases. Once triggered Hg^{2+} ions into **S16** significantly the fluorescence turn-on behavior was observed and the calculated detection limit was to be 3.4 nM (Fig. 23).

An anthracene-based fluorescent sensor **S17** exhibited novel AIE characteristics in H_2O-THF mixtures at high water content and reported for Hg^{2+} ions [36]. In THF solution, **S17** exhibits a weak fluorescence emission at 498 nm ($\Phi = 0.002$). It was observed that aggregation switched on in mixed aqueous media (THF/H_2O) by varying the volume of water percentages gradually. Increasing the volume of H_2O fractions up to 70% in the binary solvent mixture (THF/H_2O) at 518 nm shows enhanced fluorescence and simultaneously the colorless non-fluorescent solution changed to the strong fluorescent green color solution. A strong fluorescence quenching of **S17** was observed in the presence of Hg^{2+} ions via a complex interplay through the ground state complexation between **S17** and Hg^{2+} ions and external heavy atom induced perturbation by Hg^{2+} ions to the excited states of the **S17** (Fig. 24).

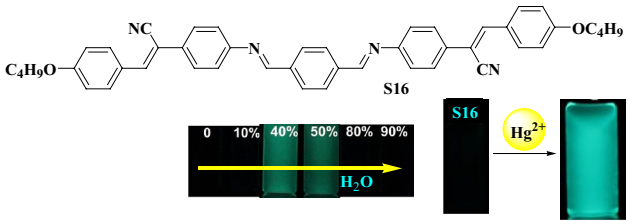

Fig. 23 Structure of **S16**

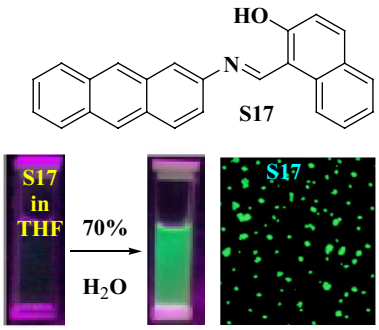

Fig. 24 Structure of **S17**

Intramolecular charge transfer (ICT) based Hg^{2+} ions detection

Intramolecular charge transfer (ICT)-based molecules require both electron-donating and electron-accepting groups conjugated into one molecule that gives rise to a

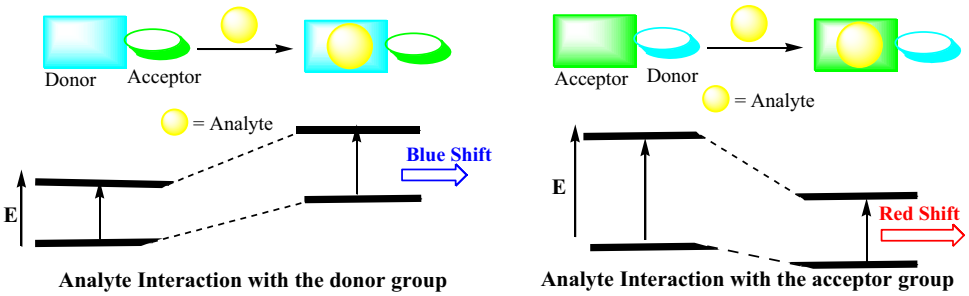

Fig. 25 Intramolecular charge transfer mechanism (ICT)

'push–pull' π-electron system in the excited state. ICT mechanisms have been widely used for cation sensing. Intramolecular charge transfer (ICT) involves an excited molecule and a neighboring molecule; one serves as an acceptor and the other as a donor molecule, involving charge redistribution in the excited molecule which produces a very large excited-state dipole moment. Upon excitation of the fluorophore, redistribution of electron density occurs so that a substantial dipole is created, resulting in intramolecular charge transfer from the donor to the acceptor. The electron donor (D) group interacts with an analyte, reducing the ICT process due to decreased electron-donating capacity, which leads to a blue shift in the absorption spectrum. In contrast, when analytes bind with the electron acceptor (A) group, an apparent red shift is observed in the absorption spectrum due to the increased ICT process [37]. Most of the fluorescent molecules are derived from the ICT mechanism by changing either the π-conjugation degree, electron-donating, or electron-withdrawing ability to interact with the target analyte (Fig. 25).

Thioacetal modified pyrene-based fluorescent sensor **S18** was reported for selective and sensitive recognition of Hg^{2+} ions in the aqueous medium over the other ions [38]. The emission spectra of **S18** are recorded in ethanol/PBS (2:1, v/v) solution and exhibits a strong fluorescence emission intensity centered at 457 nm ($\Phi = 0.33$). The fluorescence emission of **S18** (red shift) is due to the intramolecular charge transfer (ICT) mechanism in polar solvents. Upon the addition of Hg^{2+} ions into **S18**, the fluorescence intensity at 457 nm increased gradually (100-fold). The limit of detection of **S18** towards Hg^{2+} ions is determined to be 1.49 nM. The ^{1}H NMR titrations are confirmed the thioacetal moiety in **S18** can be converted to an aldehyde group upon the addition of Hg^{2+} ions (Fig. 26).

A novel acenaphtoquinoxaline-based fluorescent sensor **S19** was successfully synthesized and act as a selective fluorescent sensor for Hg^{2+} ions in acetonitrile [39]. In the presence of various metal ions such as Ba^{2+}, Ca^{2+}, Cd^{2+}, Cs^{+}, Co^{2+}, Cr^{3+}, Fe^{3+}, Fe^{2+}, Hg^{2+}, K^{+}, Li^{+}, Mg^{2+}, Mn^{2+}, Na^{+}, Ni^{2+}, Sr^{2+}, Hg^{2+} and Zn^{2+} into **S19**, an enhanced fluorescence emission intensity (red shift) is observed at 520 nm only in the presence of Hg^{2+} ions over other ions.

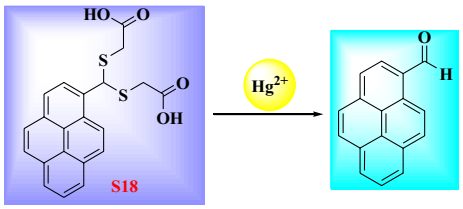

Fig. 26 Structure of **S18**

Fig. 27 Structure of **S19**

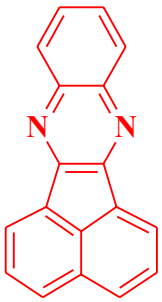

S19

The detection limit was as low as 42 ppb. The binding stoichiometry between **S19** and Hg^{2+} ions was found to be 1:1. The sensing mechanism of Hg^{2+} ions towards **S19** through the intramolecular charge transfer was investigated by DFT calculations. From the results, the sensor **S19** can be considered as a highly selective and reliable chemosensor for Hg^{2+} ion detection (Fig. 27).

A novel fluorescent sensor **S20**, which contained a conjugated dicyanomethylene-benzopyran structure as fluorophore and dithia-dioxa-monoaza crown ether moiety as the receptor was developed and reported for Hg^{2+} ions detection [40]. The sensor **S20** showed an excellent selectivity and sensitivity towards Hg^{2+} ions with no significant interference from other competitive metal ions and anions. Sensor **S20** showed strong fluorescence emission intensity at 645 nm. When an Hg^{2+} ion was added, a strong fluorescence quenching was observed. The quenching of fluorescence is due to the complexation of Hg^{2+} with dithia-dioxa-monoaza crown and weakened electron-donating ability of the recognition

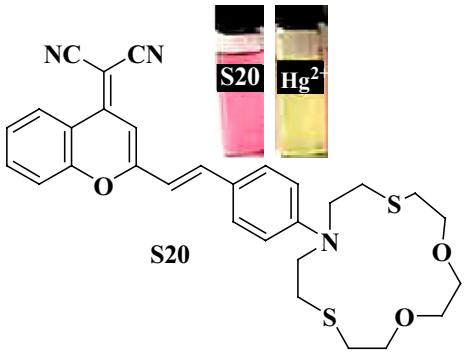

Fig. 28 Structure of **S20**

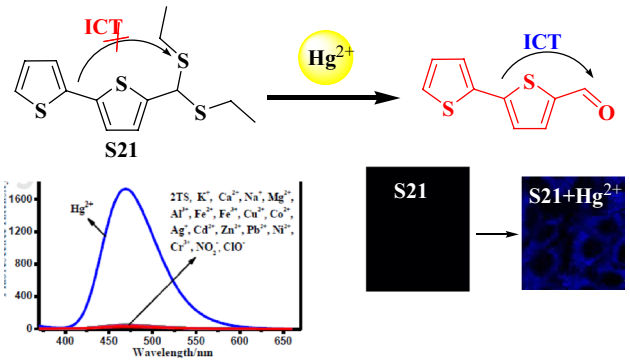

Fig. 29 Structure of **S21**

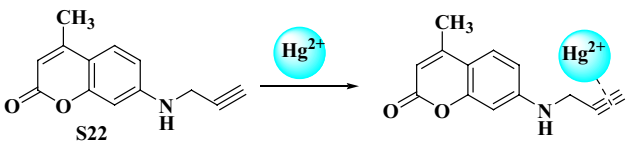

Fig. 30 Structure of **S22**

site, which resulted in the blocking of the intermolecular charge transfer (ICT) process. The fluorescence sensor **S20** was successfully used in real aqueous samples and fluorescent imaging for Hg^{2+} in living cells and zebrafish larvae with low cytotoxicity (Fig. 28).

A novel bithiophene-based fluorescent sensor **S21** was designed and developed for mercury ions detection in an aqueous medium [41]. A sequence of solutions with different ratios between ethanol and water with increasing water content (0 ~ 100%) were selected for test and finally found 100% aqueous solution is suitable for sensing action. Sensor **S21** showed a maximal absorption band at 334 nm, attributed to the absorption of bithiophene moiety. Once trigged with Hg^{2+} ions into **S21**, the appearance of a new absorbance band at 370 nm with a large red shift (36 nm). Enhanced fluorescence emission ($\Phi = 0.460$) at 470 nm was observed in

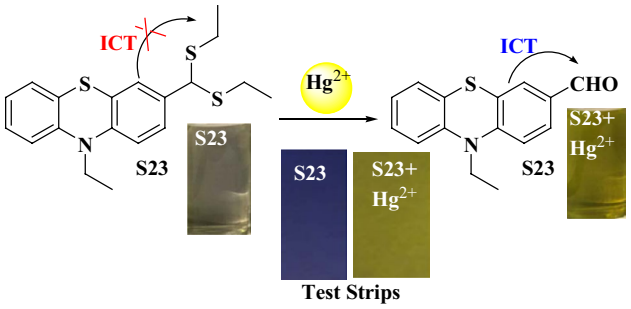

Fig. 31 Sensing mechanism of **S23** with Hg^{2+} ions

the presence of Hg^{2+} ions and an instant fluorescence color change from colorless to blue was also noted. The distinctive fluorescent enhancement signal could be recognized to the formation of new species via Hg^{2+} ions promoted dethioacetalization on **S21**, which induced the intramolecular charge transfer (ICT) process from bithiophene moiety to aldehyde group turned on. The detection limit of **S21** towards Hg^{2+} was calculated to be 19 nM (Fig. 29).

A simple and novel coumarin-based fluorescence sensor **S22** (7-(propargylamino)-4-methyl-2*H*-chromene-2-one) was designed and reported by Duan et. al., [42] for the selective and sensitive detection of Hg^{2+} ions in an aqueous solution. When excited at 350 nm, sensor **S22** displayed the greatest emission peak at 450 nm. This is due to the electrons diverted from 7-amino-4-methylcoumarin to alkynyl being blocked and the ICT process was rancid. Upon the addition of Hg^{2+} ions into sensor **S22**, the alkynyl group would be converted to keto, a comparatively strong electron-withdrawing part, which resulted in enhancement of the ICT process, and quenched the fluorescence. The fluorescent color of **S22** solutions changed from blue-green to blue under the UV (365 nm) light. Further, the sensor **S22** was successfully applied for the Hg^{2+} determinations in water samples with satisfying recovery and on agar gels (Fig. 30).

The intramolecular charge transfer based on a novel phenothiazine fluorescent sensor **S23** was designed and synthesized by simple methods [43]. Absorption spectrum sensor **S23** displayed an absorption band at 310 nm and a clear red-shifted band was observed at 390 nm upon the addition of Hg^{2+} ions. The color of sensor **S23** changed drastically from colorless to yellow (deprotection reaction) after adding the Hg^{2+} ions. When excited at 390 nm, there is an obvious fluorescence emission band at 610 nm ($\Phi = 0.115$) exhibited upon interaction with Hg^{2+} ions into sensor **S23**. The fluorescence sensor **S23** detects Hg^{2+} ions based on a deprotection reaction. In this sensor, 10-ethylphenothiazine acted as an electron donor, and 2- (demethylation) -methine was acting as a weak electron donor to form an electron donor. The donor system prevents the intra-molecular charge transfer process (ICT). In the presence of Hg^{2+} ions,

an electron-deficient aldehyde group was formed and the aldehyde group was used as the electron acceptor 10-ethylphenothiazine (Fig. 31). The detection limit was calculated to be 0.212 nM.

A novel oligothiophene-based fluorescence sensor **S24** acts as a colorimetric and ratiometric fluorescent sensor for Hg^{2+} ions based on intramolecular charge transfer (ICT) mechanism [44] in EtOH/H_2O (1:1, v/v) solution. Sensor **S24** exhibited a maximal absorption band at 360 nm (oligothiophene moiety). Upon the addition of Hg^{2+} ions into **S24**, the band at 360 nm gradually decreased and a new red-shift absorption band is formed at 400 nm along with the solution color change from colorless to pale yellow. In emission spectrum, sensor **S24** showed a blue emission band centered at 448 nm and the fluorescence enhancement intensity at 552 nm (turn-on) and a significant decrease of fluorescence intensity at 448 nm in the presence of Hg^{2+} ions. Under a UV lamp at 365 nm, the sensor **S24** solution color changed from blue to bright green. The large red shift (104 nm) and the fluorescent enhancement signals in **S24** are due to electron-rich dithioacetal moiety, which could be removed by Hg^{2+} ions to release the electron-deficient aldehyde group, and produced a strong push–pull electronic system, leading to the ICT process from oligothiophene moiety to aldehyde group being turned on (Fig. 32).

Photo-induced electron transfer (PET)-based Hg^{2+} ions detection

The photo-induced electron transfer mechanism is a deactivation process involving an internal redox reaction between the excited state of the fluorophore and another species able to donate or accept an electron. A fundamental point explaining this process is to consider that in the excited state the properties of the species are quite different compared with those of the ground state. In particular, due to its higher energy content, an excited state is both a stronger reducing and oxidant than the corresponding ground state. Generally, in fluorescent metal sensors, PET takes place from a lone pair of the coordinating atoms (e.g., N, O, S, P) to the HOMO of the excited fluorophore. The presence of a coordinated metal ion lowers the energy of the lone pair involved in the coordination preventing the PET, thus causing the switch-ON of the fluorescence. PET strongly depends on the solvent polarity, which affects the oxidation potential of the lone pairs of the coordinating moiety. Higher solvent polarities make the electron transfer easier; as a consequence, the PET-mediated quenching effect of the fluorescence occurs more quickly in high-polar environments [45]. The PET-type fluorescent response does not cause any spectroscopic shifts in the emission band upon the complexation of metal ions (Fig. 33).

A novel 7-nitrobenzo-2-oxa-1, 3-diazolyl-based fluorescence sensor **S25** containing a piperazine derivative was synthesized and developed for Hg^{2+} ions detection in a 100% aqueous medium [46]. In UV–Vis spectrum sensor **S25** shows a strong band at 495 nm due to the ICT process from the anilino group to the strong electron-withdrawing nitro group of sensor **S25**. Upon the gradual addition of Hg^{2+} ions, the ICT band at 495 nm shows a gradual increase in the absorption intensity with a blue shift. In the emission spectrum, sensor **S25** showed a very weak emission ($\Phi = 0.011$) band centered about 543 nm when excited at 495 nm. This is due to an efficient PET process from the piperazine nitrogen atom to the photo-excited sensor **S25** fluorophore. The sensor **S25** displays a significant fluorescence enhancement ($\Phi = 0.14$) toward Hg^{2+} ions through blocking of the photo-induced electron transfer process, which selectively senses Hg^{2+} ions as low as 19.2 nM (Fig. 34).

Borondipyrromethane (BODIPY)-based fluorescence sensor **S26** has been designed and developed for selective and sensitive detection of mercury ions [47]. The free sensor **S26** induces a weak emission band centered at 510 nm when excited at 496 nm ($\Phi = 0.048$). The weak emission is probably due to the efficient fluorescence quenching induced by the photo-induced electron transfer mechanism (PET) from the electron-donating amine moiety to the BODIPY framework. A strong new emission band at 514 nm with an enhancement in fluorescence intensity has appeared in the presence of Hg^{2+} ions into sensor **S26**. The fluorescence turn-on is due to the blocking of PET using Hg^{2+} ions coordination through the ether-O, pyridine-N, and amine-N of the sensor **S26** (Fig. 35).

Calix[6]arene-based fluorescence sensor **S27** has been synthesized by using p-*tert*-butylcalix[6]arene is functionalized with 5-methylfurfural and reported for a Hg^{2+} ions detection [48]. The sensor **S27** shows an absorption

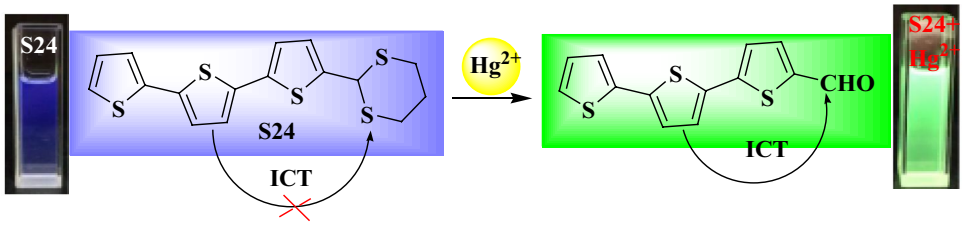

Fig. 32 Sensing mechanism of **S24** with Hg^{2+} ions

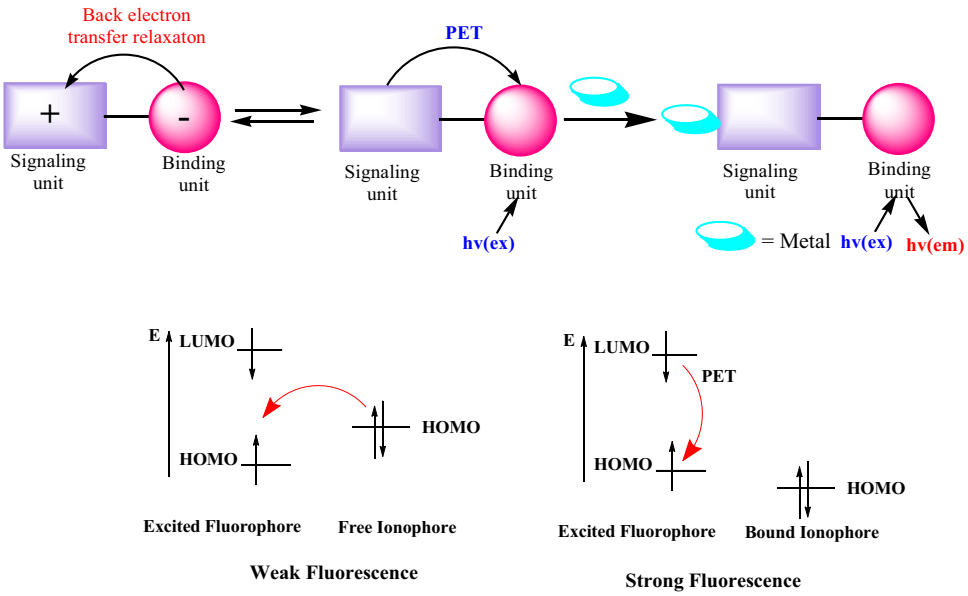

Fig. 33 Photo-induced electron transfer mechanism (PET)

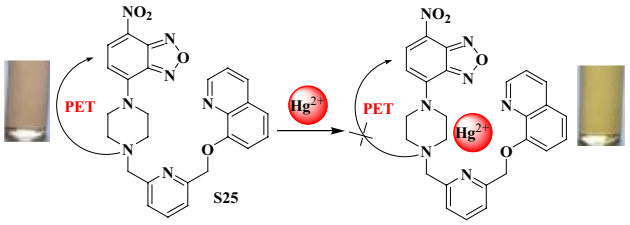

Fig. 34 Sensing mechanism of **S25** with Hg^{2+} ions

band at 303 nm. Upon the addition of Hg^{2+} ions into sensor **S27**, a new band near 326 nm with a bathochromic shift in an aqueous medium. The sensor **S27** exhibited a very weak emission band at 345 nm and this band is due to the photoinduced electron transfer (PET) mechanism. When adding Hg^{2+} ions into **S27**, significant fluorescence enhancement with bathochromic shifts was observed near 425 and 545 nm. The other ions such as K^{+}, Be^{2+}, Mg^{2+}, Ca^{2+}, Sr^{2+}, Co^{2+}, Cu^{2+}, Zn^{2+}, Cd^{2+}, Hg^{2+}, Pb^{2+}, Al^{3+}, Sb^{3+}, Eu^{3+}, Gd^{3+}, Th^{4+}, W^{4+} and U^{4+} are not interference with this sensor action. The binding constant of sensor **S27** with Hg^{2+} ions is 3.382×10^{6} M^{-1} with a 1:1 binding mode (Fig. 36).

A novel fluorescein-based fluorescence sensor **S28** was reported for highly selective and sensitivity towards Hg^{2+} ions in an aqueous medium [49]. The spectrum studies of sensor **S28** were studied in an aqueous solution (20 mM HEPES buffer, pH = 7.4). Sensor **S28** exhibited a weak fluorescence emission band of fluorescein at 529 nm when excited at 470 nm. Various metal ions such as Mn^{2+}, Fe^{2+}, Fe^{3+},Co^{2+}, Cr^{3+}, Ni^{2+}, Cu^{2+}, Zn^{2+}, Cd^{2+}, Hg^{2+}, Pb^{2+}, Ag^{+}, Mg^{2+}, Ca^{2+}, K^{+}, Na^{+}, La^{3+}, Eu^{3+}, and Er^{3+}were added to

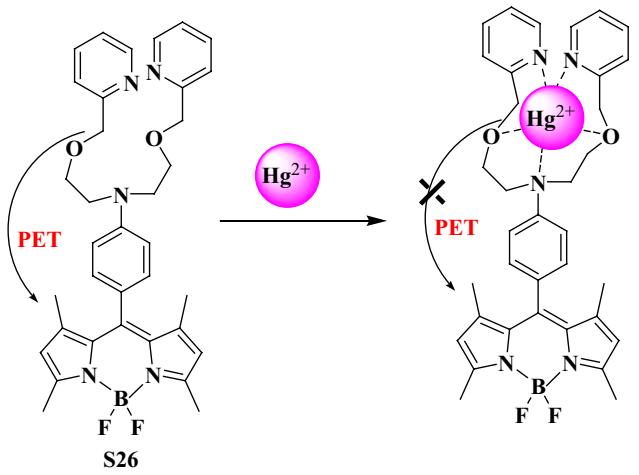

Fig. 35 Sensing mechanism of **S26** with Hg^{2+} ions

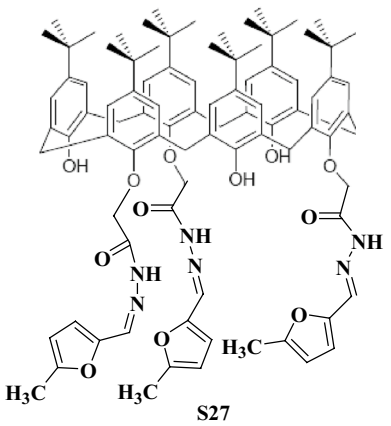

Fig. 36 Structure of **S27**

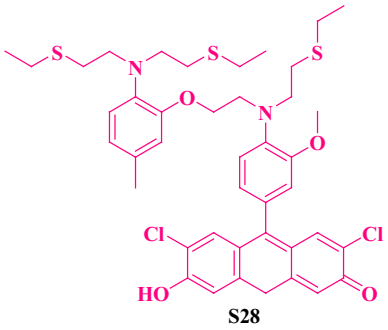

Fig. 37 Structure of **S28**

sensor **S28**, and only Hg^{2+} ions show a significant enhancement of fluorescence with the emission maximum (green color emission) at 539 nm (51-fold). The detection limit of Hg^{2+} was measured to be 22.06 ppb. The green fluorescence of the cells is similar to that of **S28**-Hg^{2+} in solution, which indicates that sensor **S28**-Hg^{2+} is membrane permeable (Fig. 37).

A novel pyridyl-based fluorescence sensor **S29** has been prepared by using a mixture of 2,6-diaminopyridine and di-2-pyridyl ketone in ethanol [50]. The sensing ability of sensor S29 in the presence of various cations such as Na^{+}, Ag^{+}, Ca^{2+}, Ba^{2+}, Cu^{2+}, Cr^{3+}, Fe^{2+}, Fe^{3+}, Co^{2+}, Hg^{2+}, Cd^{2+}, Zn^{2+}, Ni^{2+} and Pb^{2+} were studied in methanol/water solution (4:1, v/v) pH = 7.51. Sensor **S29** alone displayed two main absorption bands at 243 and 310 nm, and small absorption bands at 268 and 338 nm, which can be attributed to π–π* and n-π* transitions from the imine group. Upon the addition of Hg^{2+} ions into sensor **S29**, a bathochromic shift at 310 nm and an increase in the absorbance at 338 nm was observed due to the donor and acceptor system in the sensor **S29**, resulting in enhanced intramolecular charge transfer (ICT). The Hg^{2+} ions bind with sensor **S29,** leading to the disruption of PET, and affects decay processes of the excited states in the systems with unbound lone pair of an electron in the vicinity of the fluorophore. Enhanced emission intensity was prominent in the presence of Hg^{2+} ions with sensor **S29** since a non-radioactive decay of the excited state was inhibited (Fig. 38).

Fig. 38 Structure of **S29**

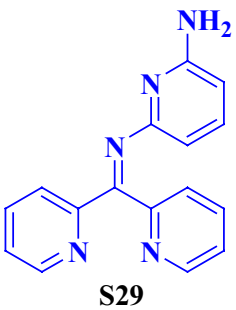

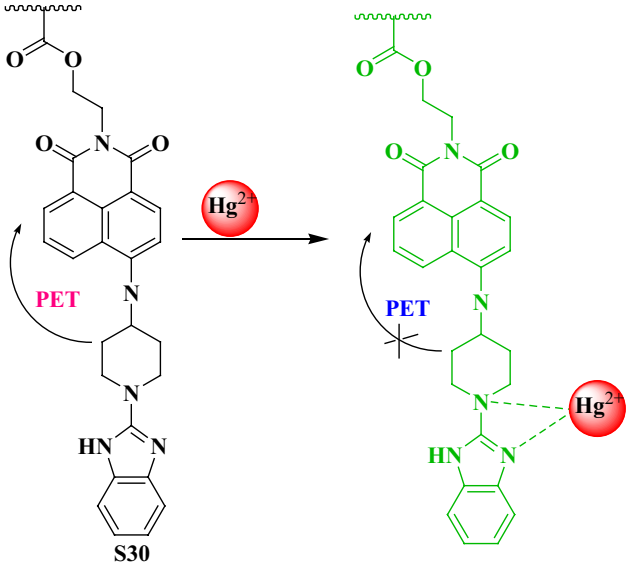

Fig. 39 Sensing mechanism of **S30** with Hg^{2+} ions

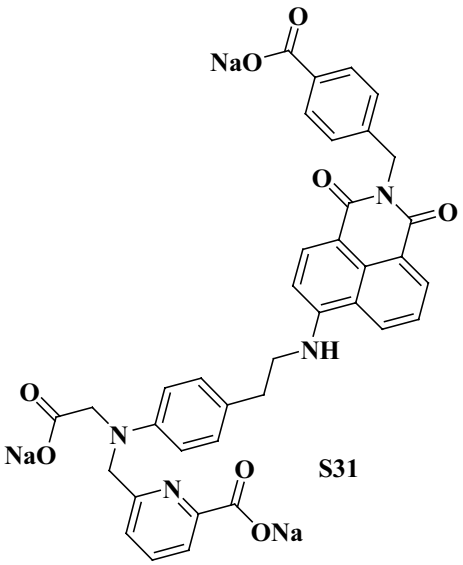

Fig. 40 Structure of **S31**

The naphthalimide-based fluorescence solid sensor **S30** has been developed by inserting *N*-(2-hydroxyethyl)-4-(4-(1*H*benzo[d] imidazol-2-yl) methyl) piperazine-1-yl)-1,8-naphthalimide to a photocrosslinked membrane reaction through the acid chloride groups [51]. The sensor **S30** was reported for selective and sensitive detection of mercury ions over other interference metal ions. Upon the addition of Hg^{2+} ions into **S30**, the effective fluorescence intensities were significantly enhanced caused by Hg^{2+} ions interaction and the formation of a sensor **S30**-Hg complex. The resulting fluorescence sensor **S30** undergoes fluorescence

Fig. 41 Structure of **S32**

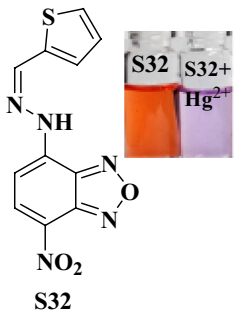

enhancement upon binding Hg^{2+} ions which aggravates a photo-induced electron transfer (PET) inhibition process from the piperazine to the naphthalimide moiety.

The limit of detection was calculated to be 0.73 nM (Fig. 39).

Another naphthalimide-based fluorescence sensor, **S31**, has been synthesized and reported for Hg^{2+} ions in aqueous solution selectively and sensitively [52]. The emission properties of the sensor **S31** were evaluated in an aqueous solution (20 mM HEPES buffer, pH = 7.4). Sensor **S31** exhibited an emission band at 550 nm (4-amino-1, 8-naphthalimide) with a weak green color emission. The addition of Hg^{2+} ions to sensor **S31**, the iminodiacetic acid, and picolinic acid as a metal chelating group caused a remarkable fluorescence enhancement (25-fold) at 550 nm. This fluorescence change is due to the energy level of the iminodiacetic acid and picolinic acid moiety being lower than that of the HOMO of the excited 4-amino-1, 8-naphthalimide, the electron transfer is not energetically favored, so the fluorescence is "switched on". The binding constant of sensor **S31** with Hg^{2+} ions was measured to be 1.46×10^8 M^{-1} with 1:1 binding mode (Fig. 40).

A novel Hg^{2+} ion sensor **S32** based on 7-nitrobenzo-2-oxa-1,3-diazolyl fluorophore connected with thiophene ionophore was prepared and reported by Kraithong and coworkers [53]. Fluorescence sensor **S32** showed a high selectivity toward Hg^{2+} ions in aqueous acetonitrile solutions and the color change of sensor **S32** changed from orange to purple. Sensor **S32** exhibited weak fluorescence at 587 nm ($\lambda_{ex} = 520$ nm), which could be attributed to the presence of the thiophene group, which led to fluorescent quenching via photoinduced electron transfer (PET) from a sulfur atom of the thiophene moiety. When increasing the concentration of Hg^{2+} ions into **S32**, the fluorescence enhancement (50-fold) was observed at 587 nm. This fluorescence turn "OFF–ON" of sensor **S32** was caused by the interaction between a sulfur atom of the thiophene ionophore and Hg^{2+} ions, which led to inhibition of the PET process upon binding of Hg^{2+} ions (Fig. 41).

Thiocarbohydrazide-based Schiff base fluorescence sensor **S33** act as a selective colorimetric and fluorescent sensor for Hg^{2+} ions over other interference ions such as Al^{3+}, Ag^{+}, Ba^{2+}, Ca^{2+}, Cd^{2+}, Co^{2+}, Cu^{2+}, Cr^{3+}, Fe^{3+}, K^{+}, Mg^{2+}, Mn^{2+}, Na^{+}, Ni^{2+}, Pb^{2+}, Hg^{2+}, Zn^{2+}, Th^{4+}, and Bi^{3+} ions [54]. Sensor **S33** consists of an electron donor triphenylamine center and electron acceptor thiourea unit. The interaction of **S33** with Hg^{2+} ions in CH_3CN: H_2O (6:4, v/v) results in a color change from colorless to yellow. In absorption studies, a new peak appeared at 386 nm (red shift) upon interaction with Hg^{2+} ions into **S33**. The sensor **S33** shows an emission band at 485 nm upon excitation at 375 nm and the band was found to be quenched completely when interacting with Hg^{2+} ions. These changes may be due to combined chelation enhanced quenching (CHEQ) and a strong photo-induced electron transfer (PET) mechanism. The limit of detection for Hg^{2+} ions was found to be 1.26 nM (Fig. 42).

Pyrenylthioureayl alanine-based fluorescence sensor **S34** was prepared by a simple condensation reaction of 3-amino pyrene with isothiocyanyl alanine in CH_3CN: DCM (1:3) solvent at 50 °C and reported for the detection of the Hg^{2+} ions [55]. Upon the addition of various metal ions such as Mg^{2+}, Mn^{2+}, Fe^{3+}, Co^{2+}, Ni^{2+}, Zn^{2+}, Ag^{+}, Cu^{+}, Cd^{2+}, Pb^{2+}, Hg^{2+}, and Cu^{2+} ions to the sensor **S34**, a slight blue shift of pyrenyl absorption bands along with a new band at 359 nm was observed only in the presence of Hg^{2+} ions. The enhancement of emission intensity was found in the presence of **S34**-Hg^{2+} ions upon excitation at 342 nm. The detection limit is found to be 93 nM and a 1:2 metal–ligand complexation possibly via the coordination with the S atom of the thiourea unit (Fig. 43).

Mercaptosuccinic acid capped CdTe/ZnS core/shell quantum dots **S35** have been synthesized and reported for selective detection of Hg^{2+} ions in an aqueous medium [56]. Quantum dots **S35** having a shell material with a wider band gap than that of the core material causes the improvement of the confinement of electrons and holes in the low band gap core. Upon the addition of Hg^{2+} ions to sensor **S35** ($\lambda^{ex} = 400$ nm), a significant fluorescence quenching was observed and this intensity decreases due to the

Fig. 42 Sensing mechanism of **S33** with Hg^{2+} ions

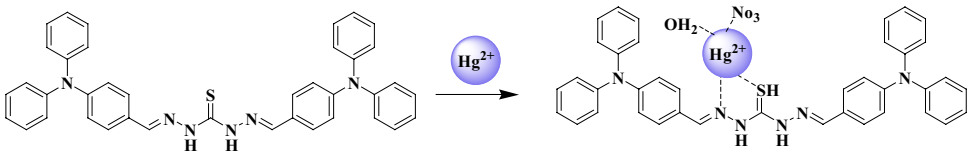

S33

Fig. 43 Structure of **S34**

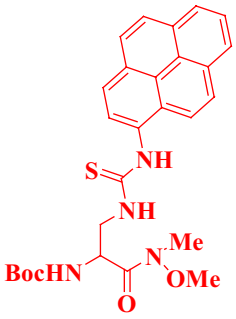

S34

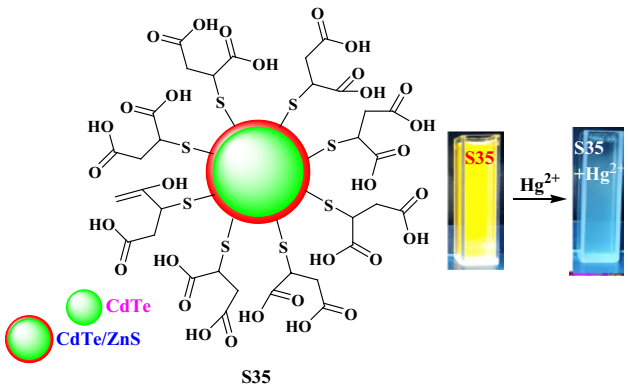

S35

Fig. 44 Structure of **S35**

photoinduced electron transfer (PET) between sensor **S35** and Hg^{2+} ions. The detection limit of sensor **S35** with Hg^{2+} ions was calculated to be 1 pM, which is remarkably less than the tolerance limit of mercury. The real-time analysis was further carried out with drinking water and tap water solutions and the sensor **S35** show remarkably good quenching in these solutions (Fig. 44).

A novel fluorescent sensor **S36** based on a metal–organic framework/DNA hybrid system was developed and reported for Hg^{2+} ions detection in an aqueous medium [57]. The fluorescence intensity decreased rapidly along with the UiO-66-NH_2 concentration ranging from 0–0.15 μg $μl^{-1}$. In the presence of Hg^{2+} ions, UiO-66-NH_2 showed a fluorescence enhancement band at 518 nm in Tris–HCl buffer (pH 7.4) medium. The detection limit was calculated to be 17.6 nM. The other metal ions such as Ca^{2+}, Cd^{2+}, Co^{2+}, Cu^{2+}, Fe^{2+}, Fe^{3+}, Mg^{2+}, Mn^{2+}, Ni^{2+}, and Pb^{2+} only showed a slight response and indicated that the sensor possesses an excellent selective signal towards Hg^{2+} with respect to other metal ions (Fig. 45).

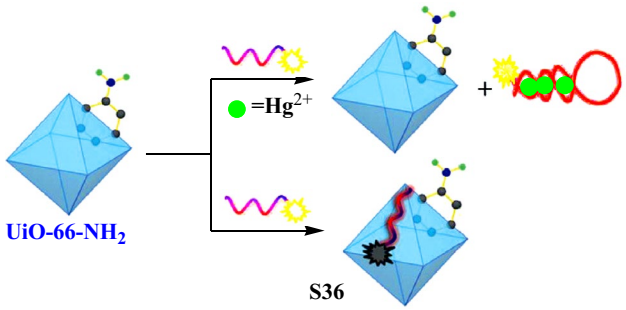

Fig. 45 Sensing mechanism of **S36** with Hg^{2+} ions

The novel fluorescent sensor **S37** was constructed by polyaniline nanoclips (PANCs) embedded with FAM-ssDNA and reported for sensitive and selective detection of Hg^{2+} ions [58]. The FAM-ssDNA has an absorption band at 495 nm (n-π* electronic transition). When polyaniline nanoclip concentration is increased, the absorption band became saturated due to the intermolecular interaction. Upon the addition of Hg^{2+} ions, it leads to retaining the absorption band due to the dissociation of FAM-ssDNA. FAM-ssDNA has shown an emission peak with high emission intensity and in the presence of polyaniline nanoclips the fluorescence intensity effectively turns off due to photo-induced electron transfer (PET). Upon the addition of Hg^{2+} ions into the sensor **S37**, Hg-induced nucleobases of FAM-ssDNA and interacted with Hg^{2+} via hydrogen bonds. The LOD was calculated to be 4 nM (Fig. 46).

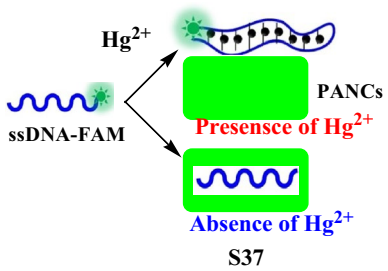

Fig. 46 Sensing mechanism of **S37** with Hg^{2+} ions

Bhatti and coworkers reported a water-soluble *p*-sulphonatocalix[4]arene appended with rhodamine fluorescence sensor **S38** for selective detection of Hg^{2+} ions over the other metal ions such as Pb^{2+}, Cu^{2+}, Zn^{2+}, Cr^{3+}, Ni^{2+}, Co^{2+}, Al^{3+}, Cd^{2+}, and Fe^{2+} ions [59]. Upon the incremental addition of Hg^{2+} ions into sensor **S38,** a distinct increase in fluorescence intensity was observed. This effect can be explained based on the electron transfer process, whereas sensor **S38** is functionalized with $N(CH_2CH_2NH_2)_3$ structure, which possesses nonbonding electrons and PET process overcome due to intermolecular oxidation process. Upon addition of Hg^{2+} ions, the intramolecular PET fluorescence quenching effect derived from the electron pairs of N donor atoms was fully blocked and relieved by reducing the electronic density of lone pairs through metal–donor binding interaction and consequently increases the sensor emission. The detection

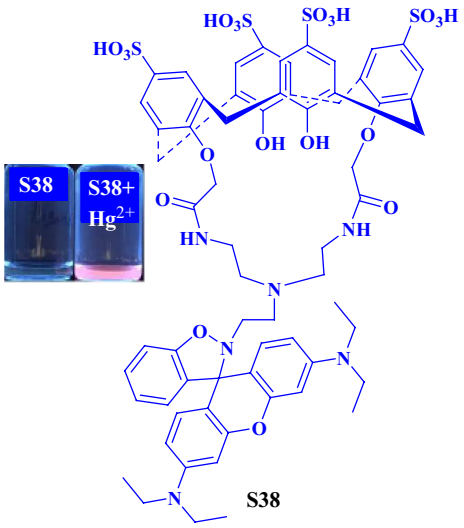

Fig. 47 Structure of **S38**

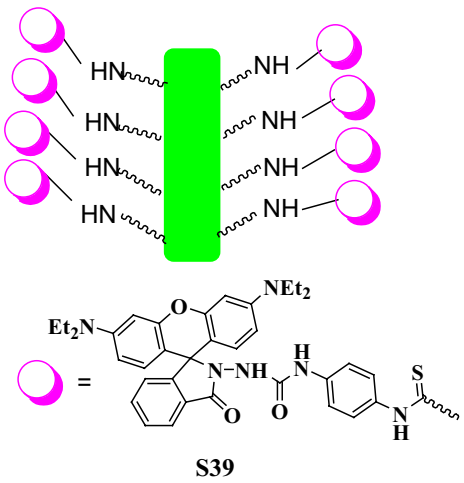

Fig. 48 Structure of **S39**

limit of sensor **S38**-Hg^{2+} was found to be 3.55×10^{-13} mol L^{-1} and the stoichiometry of complex to be 1:1 (Fig. 47).

Ring-opening mechanism-based Hg^{2+} ion detection

The fluorescence sensor **S39** based on rhodamine immobilized electrospun chitosan nanofibrous material has been developed and reported for mercury ion detection [60]. In the presence of various competing ions such as Ni^{2+}, Pd^{2+}, Zn^{2+}, Mg^{2+}, Hg^{2+}, Pb^{2+}, Fe^{2+}, Cu^{2+}, Co^{2+}, Cr^{2+}, and Cd^{2+} ions, only the addition of Hg^{2+} ions shows an enhanced fluorescence intensity. This enhanced fluorescence is due to the opening of the spirolactam ring of the rhodamine unit followed by cyclization. Sensor **S39** has a high surface area of nanofibers and provides a high number of functional groups. A divergent change in fluorescence emission from colorless to red-pink under 366-nm UV light was obtained for the sensor **S39** in the presence of Hg^{2+} ion addition (Fig. 48).

A novel fluorescence sensor **S40** based on 1,2,3-triazole and its rhodamine B derivative has been developed for the Hg^{2+} ions sensor [61]. The sensing behavior of sensor **S40** towards various metal ions such as Pb^{2+}, Mn^{2+}, K^{+}, Na^{+}, Ag^{+}, Ca^{2+}, Cd^{2+}, Co^{2+}, Cu^{2+}, Fe^{3+}, Zn^{2+}, Ni^{2+}, Hg^{2+}, Li^{+} and Mg^{2+} was studied in DMF/H_2O (v/v = 1:1, Tris–HCl, pH = 7.4) solutions. Sensor **S40** alone displayed a non-emissive spectrum, which indicated the rhodamine moiety in ring-closed spirolactam form. Upon the addition of the Hg^{2+} ion, an enhanced fluorescence emission band (4500-fold) at 584 nm (λ_{ex} = 563 nm) was observed. Simultaneously, the color of sensor **S40** solution changed from colorless to pink in the presence of Hg^{2+} ions. The enhanced fluorescence change is due to ring-opening from the spirolactam (**S40**) to a ring-opened amide. The fluorescence imaging of Hg^{2+} ions in HeLa cells was successfully applied in sensor **S40** and demonstrates a good membrane-permeable reagent for biological imaging applications (Fig. 49).

Rhodamine-bearing cage-like silsesequioxanes-based fluorescence sensor **S41** has been developed for Hg^{2+} ions in 10% aqueous ethanol solutions [62]. With the addition of increasing concentration of Hg^{2+} ions, a new absorption band significantly appeared at 555 nm at the same time. The colorless sensor **S41** solution changed to pink color. When excited at 520 nm, the solution of sensor **S41** showed a weak fluorescence signal (turn off). Upon the addition of Hg^{2+} ions, the intensity of the fluorescence emission was rapidly enhanced, and "turn on" fluorescence intensity was observed at 580 nm corresponding to the spirolactam ring opened-form of rhodamine fluorophores and the detection limit was found to be 0.63 ppb (Fig. 50).

Rhodamine 6G-based fluorescence sensor **S42** has been synthesized by using rhodamine hydrazide, anhydrous triethylamine, and a solution of triphosgene in dichloromethane and applied for selective detection of Hg^{2+} ions in ethanol/water (1/1 v/v) solutions [63]. The fluorescence spectra of sensor **S42** exhibited very weak fluorescence intensity at 561 nm, which is attributed to the colorless and non-fluorescent spirocyclic form of rhodamine. Among the addition of various metal ions, only the Hg^{2+} ions alone showed a high fluorescence enhancement band at 561 nm and the color of the sensor **S42** solution changed from colorless to pink. Sensor **S42** has an excellent specificity for Hg^{2+} ions and a very low detection limit of 1.3 ppb. Fluorescence bio imaging shows that sensor **S42** has good cell membrane permeability and can be applied to monitor intracellular Hg^{2+} ions in living cells, animal tissues, and plant tissues (Fig. 51).

Three novel rhodamine fluorescence sensors **S43a-c** act as a selective colorimetric and fluorescence sensor for Hg^{2+} ions in Tris—HCl/C_2H_5OH (v: v = 3: 7, 10 mM, pH = 7.2)

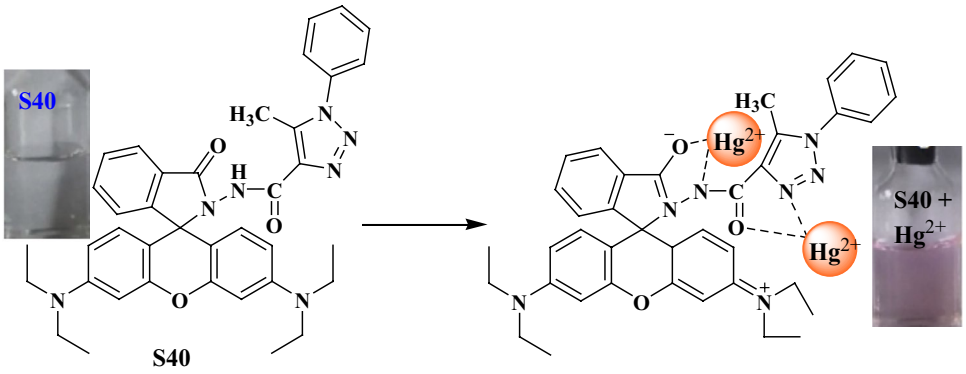

Fig. 49 Sensing mechanism of **S40** with Hg^{2+} ions

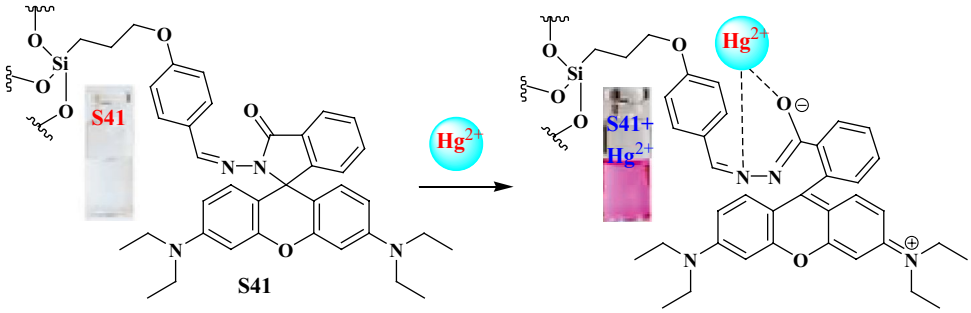

Fig. 50 Sensing mechanism of **S41** with Hg^{2+} ions

[64]. Colorless sensors **S43a-c** are turned to pink color once they interact with Hg^{2+} ions. Upon the incremental addition of Hg^{2+} ions into sensors, a strong fluorescence enhancement was observed at 576 nm (20-fold) and also noted that the colorless sensors solutions changed to orange-red under UV irradiation. This fluorescence enhancement is due to a ring-opening of the spirolactam unit after coordination with sensors **S43a-c** and the paramagnetic effect of the Hg^{2+} ions. The binding constants between sensors **S43a-c** and Hg^{2+} are 5.0×10^{6} M^{-1}, 1.8×10^{6} M^{-1}, 1.5×10^{6} M^{-1}, respectively. The other cations and anions such as Cd^{2+}, Co^{2+}, Cr^{3+}, Cu^{2+}, Mn^{2+}, Ni^{2+}, Zn^{2+}, Pb^{2+}, Fe^{3+}, Ag^{+}, Ba^{2+}, Bi^{3+}, Sr^{+}, Na^{+}, K^{+}, Ca^{2+}, Mg^{2+}, $H_2PO_4^{-}$, HPO_4^{2-}, PO_4^{3-}, SO_4^{2-}, $C_2O_4^{2-}$, CO_3^{2-}, ClO^{-}, NO_3^{-}, NO_2^{-}, SCN^{-}, Ac^{-}, F^{-}, Cl^{-}, Br^{-}, I^{-}, CN^{-}, HSO_4^{-} ions did not show any changes in naked-eye and fluorescence emission peaks. The limits of detections (LOD) were calculated to be 18, 16, and 56 nM, respectively (Fig. 52).

Xu and coworkers reported a simple fluorescence sensor **S44** for Hg^{2+} ion detection [65]. The sensor **S44** was prepared by reaction of rhodamine B hydrazide with 2-amino-4-ferrocenylthiazole and applied for molecular recognition studies with analytes. A significant absorbance band was noticed at 560 nm upon the addition of Hg^{2+} ions. No significant emission response was observed after the addition of other metal ions such as Mn^{2+}, Co^{2+}, Ni^{2+}, Hg^{2+}, Fe^{2+}, Na^{+}, Sr^{2+}, Cu^{2+}, K^{+}, Ba^{2+}, Ca^{2+}, Mg^{2+}, Zn^{2+}, Al^{3+}, Fe^{3+}, Cd^{2+}, and Cs^{+} ions. Sensor **S44** shows a weak fluorescence emission band when exciting the sensor. Upon the addition of

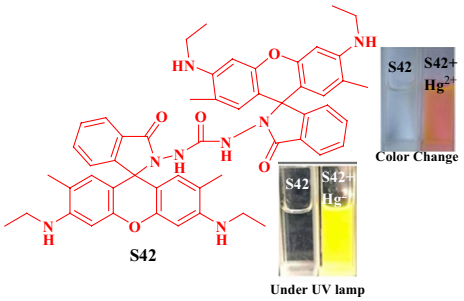

Fig. 51 Structure of **S42**

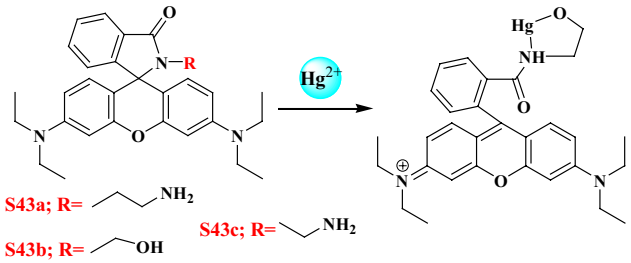

Fig. 52 Sensing mechanism of **S43** with Hg^{2+} ions

Hg^{2+} ions to sensor **S44**, a new fluorescence enhanced band positioned at 621 nm in addition to color change from colorless to pink was observed by the naked eye. This enhancement is mainly due to the spirolactam ring of rhodamine

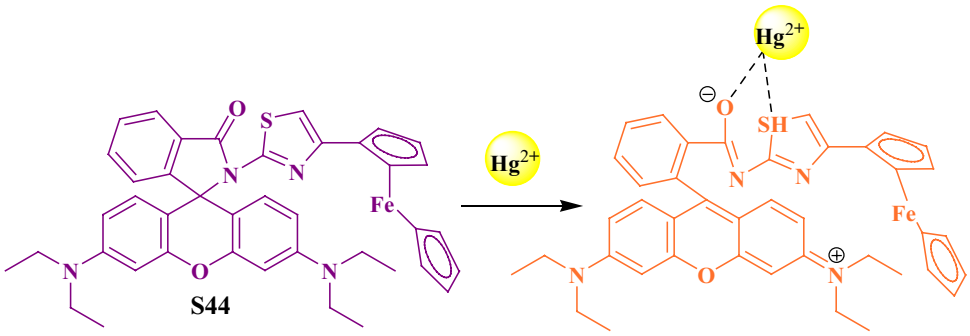

Fig. 53 Sensing mechanism of **S44** with Hg^{2+} ions

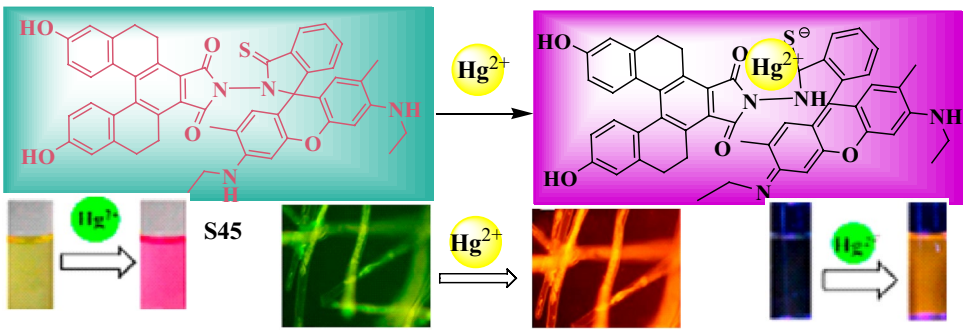

Fig. 54 Sensing mechanism of **S45** with Hg^{2+} ions

opening when Hg^{2+} ions coordinate with sensor **S44**. The detection limit was calculated to be as low as 0.53 μM with a 1:1 binding coordination ratio (Fig. 53).

Rhodamine 6G bearing [5]Helicene dye-based hybrid fluorescent sensor **S45** was synthesized successfully [66] and reported for the detection of Hg^{2+} ions in HEPES buffer/methanol solution (1:1 v/v, 5 mM, pH 7.2). The color of sensor **S45** solution was yellow and exhibited absorption peaks at 310 and 373 nm. Upon the addition of Hg^{2+} ions, the absorption band at 535 nm increased significantly and the yellow color **S45** solution turned to pink. These changes are mainly due to the mercury-promoted spirolactam ring-opening behavior. Weak fluorescence intensity of sensor **S45** was observed at 560 nm when exciting the solution at 373 nm. Upon the incremental addition of Hg^{2+} ions, a notable fluorescence enhancement ($\Phi = 0.53$) was observed via the FRET process and displayed a non-fluorescent color to orange fluorescence. The FTIR studies revealed that Hg^{2+} bonded with the oxygen atoms of imine of [5]helicene-like imide and sulfur atom of rhodamine thioamide of sensor **S45** (Fig. 54).

Rhodamine-based fluorescence sensor **S46** was developed and synthesized for Hg^{2+} ions detection in THF/H_2O (9:1, v/v) solution [67]. Sensor **S46** displayed selective sensing of Hg^{2+} ions and showed a color change from colorless to pink color in solution state and red to pink color in solid-state. The sensor **S46** displayed a very weak single fluorescence emission band at 400 nm. Upon addition of Hg^{2+} ions, sensor **S46** exhibited a prominent fluorescence enhancement

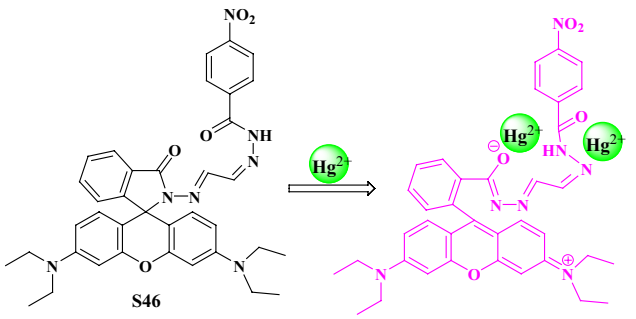

Fig. 55 Sensing mechanism of **S46** with Hg^{2+} ions

with a red shift band observed at 570 nm (16 fold). The addition of Hg^{2+} ions leads the spirocycle unit open via coordination, resulting in color change and the generation of a strong fluorescence. The association constant of the **S46**-Hg^{2+} complex was calculated to be 8.25×10^9 M^{-1}, and the detection limit for Hg^{2+} ions was found to be 27 ppb (Fig. 55).

A novel rhodamine-6G-based fluorescence sensor **S47** [68] acts as a highly selective fluorescence sensor for Hg^{2+} ions in HEPES buffer (10 mM, pH-7.4)/CH_3CN (40:60, V/V). The colorless sensor **S47** shows a dramatic yellow color and displayed a new absorption peak that appeared at 533 nm in the presence of Hg^{2+} ions. The other cations are not in interference with the color change as well as in spectral changes. When increasing the Hg^{2+} ion concentration, the fluorescence emission spectra of sensor **S47**

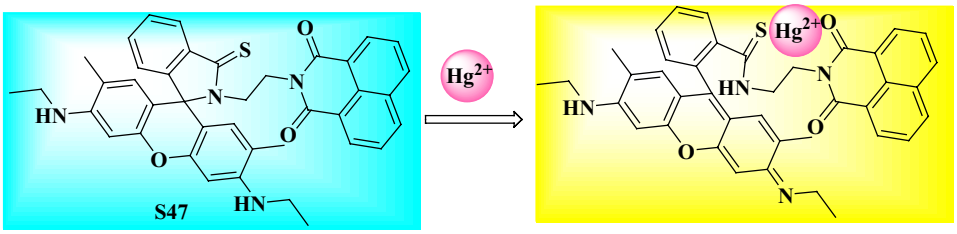

Fig. 56 Sensing mechanism of **S47** with Hg^{2+} ions

changed significantly, where the emission peak appeared at 560 nm. The enhancement may be due to the structure of sensor **S47** transformation from spirolactam to the ring-opened amide form with adding Hg^{2+} ions. The practical application of sensor **S47** towards Hg^{2+} ions was investigated in test strips and shows an obvious color change in strips (Fig. 56).

A simple sensor **S48** based on p-*tert*-butylcalix[4]arene thiospirolactam rhodamine b acts as a fluorescence sensor for Hg^{2+} ions [69]. The sensing studies towards sensor **S48** with metal ions such as Ag^{2+}, Ba^{2+}, Ca^{2+}, Co^{2+}, Cd^{2+}, Cu^{2+}, Fe^{2+}, Fe^{3+}, K^{+}, Mn^{2+}, Mo^{2+}, Na^{+}, Ni^{2+}, Sn^{2+}, Sr^{2+}, Zn^{2+} and Hg^{2+} were investigated. Except for Hg^{2+}, the other ions did not interfere in the molecular recognition studies, and this confirms the sensor **S48** sense Hg^{2+} ions selectively and sensitively in ethanol–water (v/v 8/2, Tris–HCl 20 mM pH = 7.0). The colorless solution of sensor **S48** changed to pink color in the presence of Hg^{2+} ions. When the concentration of Hg^{2+} ion increases, there is an appearance of a new peak at 562 nm with a slight red shift. The appearance of the new peak may be due to the thiospirolactam ring opening of rhodamine caused by the Hg^{2+} ion. Sensor **S48** shows an emission maximum at 430 nm (0.079) due to the spirolactam structure of rhodamine moiety. In the presence of Hg^{2+} ions, the enhanced emission fluorescence intensity was observed at 582 nm (0.082) and this peak is responsible for spirolactam ring opening. Sensor **S48** is successfully penetrated the HeLa cells and gives fluorescence quantification of Hg^{2+} ions under biological conditions (Fig. 57).

A novel rhodamine-based fluorescence sensor **S49** was reported [70] for Hg^{2+} ions detection in CH_3CN/HEPES buffer (1/99, v/v, pH = 7.05). Upon addition of various interference metal ions into sensor **S49**, only Hg^{2+} exhibited a new absorption band centered at 561 nm along with a clear color change from colorless to red. Further, the emission studies of sensor **S49** towards Hg^{2+} ions were studied in an aqueous solution. Upon the addition of Hg^{2+} ions, a remarkable enhancement of the fluorescence intensity was noticed at 578 nm (170-fold) with an emerging brilliant orange fluorescence. These results indicated that Hg^{2+} ions induced the ring-opening of spirolactam in sensor **S49** and sensor

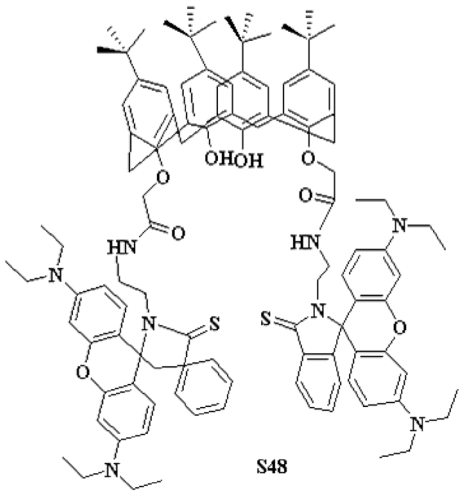

Fig. 57 Structure of **S48**

S49 might be a highly selective and sensitive colorimetric and fluorescent sensor for Hg^{2+}. The detection limit of sensor **S49** towards Hg^{2+} ions was calculated to be 0.14 µM (Fig. 58).

A novel non-sulfur rhodamine derivative with an ethylene moiety-based sensor **S50** selectively and sensitively sense Hg^{2+} ions in acetonitrile [71]. The free sensor **S50** is colorless in CH_3CN, showing almost no absorption at approximately 450–650 nm. Upon the addition of tested metal ions, only Hg^{2+} leads to a color change to pink and exhibited a strong absorption band at 557 nm (Fig. 57). When exciting the sensor **S50** at 525 nm, no significant fluorescence emission was detected between 535 and 650 nm. These interpretations indicate that the sensor **S50** exists as a non-fluorescent spirocyclic form. The Hg^{2+} ion displays strong fluorescence enhancement (640-fold) with the maximum emission at 584 nm ($\Phi = 0.25$). The fluorescence enhancement of **S49**-Hg^{2+} is due to the coordination of Hg^{2+} to the ethylene moiety and oxygen atom of the carbonyl group could induce the breaking of the C–N bond in the spirocyclic ring of sensor **S50** (Fig. 59). The detection limit was determined to be 0.2 µM.

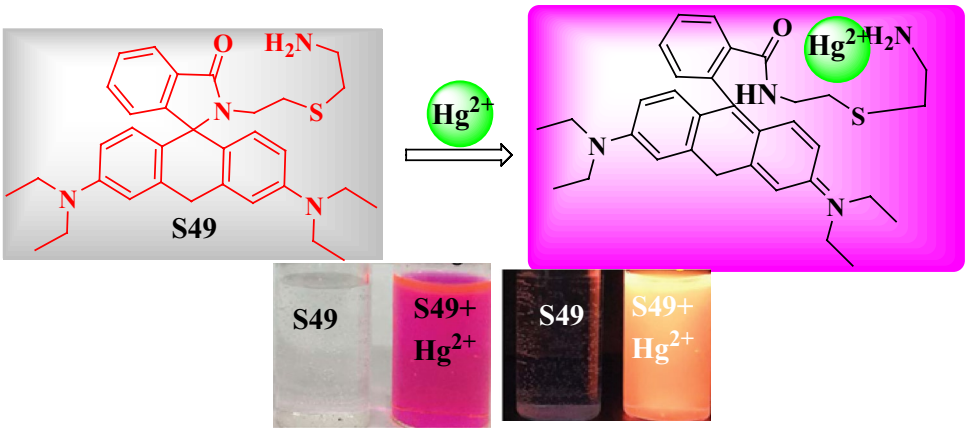

Fig. 58 Sensing mechanism of S49 with Hg^{2+} ions

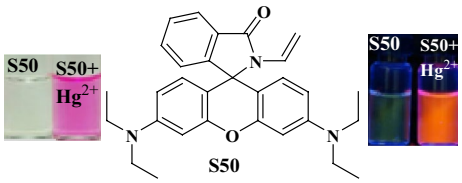

Fig. 59 Structure of **S50**

Conclusions

Mercury is one of the most toxic and heavy metal elements. Mercury contamination is extensive and occurs through various processes, e.g., volcanic emissions, mining, solid waste incineration, and in the combustion of fossil fuels. It is to be frightened that mercury-containing chemicals have been linked with a number of human health problems, including myocardial infarction, Minamata disease, damage to the brain, kidneys, and some kinds of autism, and damage to the sensory parts of the central nervous system, immune system, and endocrine system. The most common method used for the detection process of toxic and heavy Hg^{2+} ions is the chromogenic and fluorogenic reaction. The new development of fluorescence sensors that can monitor Hg^{2+} ions is very important. Fluorescent sensing is becoming a tool for molecular recognition due to its potential application in biological and environmental. Fluorescent sensors have their advantages in high sensitivity, selectivity, simplicity, low detection limit, and application to bioimaging.

This review is mainly focused on the recognition of toxic mercury ions in an aqueous medium without compromising the selectivity and sensitivity based on their sensing mechanism. However, the methods have some limitations, like low complex stability in complex matrix compounds. Conventional signaling mechanisms for the design of fluorescent chemosensors including PET, ICT, MLCT, and FRET have been widely investigated and successfully applied in a versatile range of fields during the last few years. For the past 5 years, some new mechanisms for designing fluorescence sensors have materialized to meet diverse design and application requirements. This review covers the general design principles for fluorescent sensors based on different photophysical mechanisms and recapitulates the recent advances in new mechanisms such as ring-opening and AIE for the past 5 years. On reading this tutorial review, it may seem to young researchers that all the great problems in chemosensors research have already been solved. The reported fluorescence sensor probes will help readers regarding which material should be chosen for the best design of interesting fluorescence probes with fascinating applications.

Author contributions The author confirms the sole responsibility for the manuscript preparation.

Funding No funding was received for this work.

Data availability All data underlying the results are available as part of the article and no additional source data are required.

Declarations

Conflict of interest The authors declare that they have no competing interests.

Consent for publication Not Applicable.

Ethical approval Not Applicable.

Consent to participate Not Applicable.

References

1. Liu, S., Wang, Y.M., Han, J.: Fluorescent chemosensors for copper(II) ion: structure, mechanism and application. J.

Photochem. Photobiol. C **32**, 78–103 (2017). https://doi.org/10.1016/j.jphotochemrev.2017.06.002
2. Kwon, N., Hu, Y., Yoon, J.: Fluorescent chemosensors for various analytes including reactive oxygen species, biothiol, metal ions, and toxic gases. ACS Omega **3**, 13731–13751 (2018). https://doi.org/10.1021/acsomega.8b01717
3. Wu, D., Sedgwick, A., Gunnlaugsson, T., Akkaya, E., Yoon, J., James, T.D.: Fluorescent chemosensors: the past, present and future. Chem. Soc. Rev. **46**, 7105–7123 (2017). https://doi.org/10.1039/C7CS00240H
4. Bernhoft, R.A.: Mercury toxicity and treatment: a review of the literature. J. Environ. Public. Health. **2012**, 460508 (2012). https://doi.org/10.1155/2012/460508
5. Saleh, T.A., Fadillah, G., Ciptawati, E., Khaled, M.: Analytical methods for mercury speciation, detection, and measurement in water, oil, and gas. Trends Anal. Chem. **132**, 116016 (2020). https://doi.org/10.1016/j.trac.2020.116016
6. Berhanu, A.L., Gaurav, M.I., Malik, A., Aulakh, J., Kumar, V., Kim, K.-H.: A review of the applications of Schiff bases as optical chemical sensors. Trends Anal. Chem. **116**, 74–91 (2019). https://doi.org/10.1016/j.trac.2019.04.025
7. Udhayakumari, D., Naha, S., Velmathi, S.: Colorimetric and fluorescent chemosensors for Cu^{2+}. A comprehensive review from the years 2013–15. Anal. Methods. **9**, 552–578 (2017). https://doi.org/10.1039/C6AY02416E
8. Udhayakumari, D., Velmathi, S.: Azo linked polycyclic aromatic hydrocarbons-based dual chemosensor for Cu^{2+} and Hg^{2+} ions. Ind. Eng. Chem. Res. **54**, 3541–3547 (2015). https://doi.org/10.1021/acs.iecr.5b00775
9. Zu, Y.R., Li, H., Shi, B.B., Qu, W.J., Zhang, Y.M., Lin, Q., Yao, H., Wei, T.B.: A reversible fluorescent chemosensor for the rapid detection of mercury ions (ii) in water with high sensitivity and selectivity. RSC Adv. **4**, 61320–61323 (2014). https://doi.org/10.1039/C4RA09961C
10. Samanta, T., Shunmugam, R.: Colorimetric and fluorometric probes for the optical detection of environmental Hg(II) and As(III) ions. Mater. Adv. **2**, 64–95 (2021). https://doi.org/10.1039/D0MA00521E
11. Liu, C., Chen, X., Zong, B., Mao, S.: Recent advances in sensitive and rapid mercury determination with graphene-based sensors. J. Mater. Chem. A. **7**, 6616–6630 (2019). https://doi.org/10.1039/C9TA01009B
12. Chen, G., Guo, Z., Zeng, G., Tang, L.: Fluorescent and colorimetric sensors for environmental mercury detection. Analyst. **140**, 5400–5443 (2015). https://doi.org/10.1039/C5AN00389J
13. Peakall, D.B., Lovett, R.J.: Mercury: its occurrence and effects in the ecosystem. Bioscience **22**, 20–25 (1972). https://doi.org/10.2307/1296180
14. Bishop, K., Shanley, J.B., Riscassi, A., Wit, H.A., Eklöf, K., Meng, B., Mitchell, C., Osterwalder, S., Schuster, P.F., Webster, J., Zhu, W.: Recent advances in understanding and measurement of mercury in the environment: Terrestrial Hg cycling. Sci. Total Environ. **721**, 137647 (2020). https://doi.org/10.1016/j.scitotenv.2020.137647
15. Yeoh, T.S., Lee, A.S., Lee, H.S.: Absorption of mercuric sulphide following oral administration in mice. Toxicology **41**, 107–111 (1986). https://doi.org/10.1016/0300-483X(86)90108-3
16. Mao, L., Liu, X., Wang, B., Lin, C., Xin, M., Zhang, B.T., Wu, T., He, M., Ouyang, W.: Occurrence and risk assessment of total mercury and methylmercury in surface seawater and sediments from the Jiaozhou Bay, Yellow Sea. Sci. Total Environ. **714**, 136539 (2020). https://doi.org/10.1016/j.scitotenv.2020.136539
17. Ackerman, J.T., Kraus, T.E.C., Fleck, J.A., Krabbenhoft, D.P., Horwath, W.R., Bachand, S.M., Herzog, M.P., Hartman, C.A., Bachand, P.A.M.: Experimental dosing of wetlands with coagulants removes mercury from surface water and decreases mercury bioaccumulation in fish. Environ. Sci. Technol. **49**, 6304–6311 (2015). https://doi.org/10.1021/acs.est.5b00655
18. Escudero, L.B., Olsina, R.A., Wuilloud, R.G.: Polymer-supported ionic liquid solid phase extraction for trace inorganic and organic mercury determination in water samples by flow injection-cold vapor atomic absorption spectrometry. Talanta **116**, 133–140 (2013). https://doi.org/10.1016/j.talanta.2013.05.001
19. Wang, Z., Si, S., Luo, Z., Qin, T., Xu, Z., Liu, B.: An AIE-based fluorescent probe for detection of picric acid in water **50**, 103–105 (2021). https://doi.org/10.1246/cl.200618
20. Bahta, M., Ahmed, N.: An AIEE active 1, 8-naphthalimide- sulfamethizole probe for ratiometric fluorescent detection of Hg^{2+} ions in aqueous media. J. Photochem. Photobiol. A. **391**, 112354 (2020). https://doi.org/10.1016/j.jphotochem.2020.112354
21. Silpcharu, K., Sukwattanasinitta, M., Rashatasakhon, P.: Novel sulfonamidospirobifluorenes as fluorescent sensors for mercury(II) ion and glutathione. RSC Adv. **9**, 11451–11458 (2019). https://doi.org/10.1039/C9RA00004F
22. Li, Y., Zhou, H., Chen, W., Sun, G., Sun, L., Su, J.: A simple AIE-based chemosensor for highly sensitive and selective detection of Hg^{2+} and CN^-. Tetrahedron **72**, 5620–5625 (2016). https://doi.org/10.1016/j.tet.2016.07.054
23. He, T., Ou, W., Tang, B.Z., Qin, J., Tang, Y.: In vivo visualization of the process of Hg^{2+} bioaccumulation in water flea Daphnia carinata by a novel aggregation-induced emission fluorogen. Chem. Asian J. **14**, 796–801 (2019). https://doi.org/10.1002/asia.201801538
24. Han, X., Lü, X., Chen, Z., Yu, G., Yin, J., Liu, S.: A Fluorescent probe for Hg^{2+} based on Gold(I) complex with an aggregation-induced emission feature. Chin. J. Chem. **33**, 1064–1068 (2015). https://doi.org/10.1002/cjoc.201500324
25. Ma, X.Q., Wang, Y., Wei, T.B., Qi, L.H., Jiang, X.M., Ding, J.D., Zhu, W.B., Yao, H., Zhang, Y.M., Lin, Q.: A novel AIE chemosensor based on quinoline functionalized Pillar[5]arene for highly selective and sensitive sequential detection of toxic Hg^{2+} and CN^-. Dyes Pigm. **164**, 279–286 (2019). https://doi.org/10.1016/j.dyepig.2019.01.049
26. Wang, A., Yang, Y., Yu, F., Xue, L., Hu, B., Fan, W., Dong, Y.: A highly selective and sensitive fluorescent probe for quantitative detection of Hg^{2+} based on aggregation-induced emission features. Talanta **132**, 864–870 (2015). https://doi.org/10.1016/j.talanta.2014.10.048
27. Zhang, R.X., Li, P.F., Zhang, W.J., Li, N., Zhao, N.: A highly sensitive fluorescent sensor with aggregation-induced emission characteristics for the detection of iodide and mercury ions in aqueous solution. J. Mater. Chem. C **4**, 10479–10485 (2016). https://doi.org/10.1039/C6TC03696A
28. Ruan, Z., Shan, Y., Gong, Y., Wang, C., Ye, F., Qiu, Y., Liang, Z., Li, Z.: Novel AIE-active ratiometric fluorescent probes for mercury(II) based on the Hg^{2+}-promoted deprotection of thioketal, and good mechanochromic properties. J. Mater. Chem. C. **6**, 773–780 (2018). https://doi.org/10.1039/C7TC04712F
29. Gabr, M.T., Pigge, F.C.: A turn-on AIE active fluorescent sensor for Hg^{2+} by combination of 1,1-bis(2-pyridyl)ethylene and thiophene/bithiophene fragments. Mater. Chem. Front. **1**, 1654–1661 (2017). https://doi.org/10.1039/C7QM00085E
30. Niu, C., Liu, Q., Shang, Z., Zhao, L.: Ouyang J Dual-emission fluorescent sensor based on AIE organic nanoparticles and au nanoclusters for the detection of mercury and melamine. Nanoscale **7**, 8457–8465 (2015). https://doi.org/10.1039/C5NR00554J
31. Gupta, S., Milton, M.D.: Synthesis of novel AIEE active pyridopyrazines and their applications as chromogenic and fluorogenic probes for Hg^{2+} detection in aqueous media. N. J. Chem. **42**, 2838–2849 (2018). https://doi.org/10.1039/C7NJ04573E

32. Wang, K., Li, J., Ji, S., Li, L., Qiu, Z., Pan, C., Zhang, J., Huo, Y.: Fluorescence probes based on AIE luminogen: application for sensing Hg^{2+} in aqueous media and cellular imaging. N. J. Chem. **42**, 13836–13846 (2018). https://doi.org/10.1039/C8NJ02245C
33. Singh, P.K., Prabhune, A., Ogale, S.: Pulsed laser-driven molecular self-assembly of cephalexin: aggregation-induced fluorescence and its utility as a mercury ion sensor. Photochem Photobiol. **91**, 1340–1347 (2015). https://doi.org/10.1111/php.12526
34. Wang, X., Gao, Z., Zhu, J., Gao, Z., Wang, F.: Aggregation-induced emission of cyanostilbene amphiphile as a novel platform for FRET-Based ratiometric sensing of mercury ion in water. Polym. Chem. **7**, 5217–5220 (2016). https://doi.org/10.1039/C6PY01109H
35. Fang, W., Zhang, G., Chen, J., Kong, L., Yang, L., Bi, H., Yang, J.: An AIE active probe for specific sensing of Hg^{2+} based on linearconjugated bis-Schiff base. Sens. Actuators B **229**, 338–346 (2016). https://doi.org/10.1016/j.snb.2016.01.130
36. Shyamal, M., Maity, S., Maity, A., Maity, R., Roy, S., Misra: A Aggregation induced emission based "turn-off" fluorescent chemosensor for selective and swift sensing of mercury (II) ions in water. Sens. Actuators B **263**, 347–359 (2018). https://doi.org/10.1016/j.snb.2018.02.130
37. Wang, J., Qian, X., Cui, J.: Detecting Hg^{2+} ions with an ICT fluorescent sensor molecule: remarkable emission spectra shift and unique selectivity. J. Org. Chem. **71**, 4308–4311 (2006). https://doi.org/10.1021/jo052642g
38. Gao, Y., Ma, T., Ou, Z., Cai, W., Yang, G., Li, Y., Xu, M., Li, Q.: Highly sensitive and selective turn-on fluorescent chemosensors for Hg^{2+} based on thioacetal modified pyrene. Talanta **178**, 663–669 (2018). https://doi.org/10.1016/j.talanta.2017.09.089
39. Darroudi, M., Ziarani, G.M., Ghasemi, J.B., Badiei, A.: Acenaphtoquinoxaline as a selective fluorescent sensor for Hg (II) detection: experimental and theoretical studies. Heliyon. **6**, e04986 (2020). https://doi.org/10.1016/j.heliyon.2020.e04986
40. Lv, H., Yuan, G., Zhang, G., Ren, Z., He, H., Sun, Q., Zhang, X., Wang, S.: A novel benzopyran-based colorimetric and near-infrared fluorescent sensor for Hg^{2+} and its imaging in living cell and zebrafish. Dyes Pigm. **172**, 107658 (2020). https://doi.org/10.1016/j.dyepig.2019.107658
41. Li, C., Niu, Q., Wang, J., Wei, T., Li, T., Chen, J., Qin, X., Yang, Q.: Bithiophene-based fluorescent sensor for highly sensitive and ultrarapid detection of Hg^{2+} in water, seafood, urine and live cells. Spectrochim. Acta A. **233**, 118208 (2020). https://doi.org/10.1016/j.saa.2020.118208
42. Duan, X., Gu, B., Zhou, Q., Hu, X., Huang, L., Su, W., Li, H.: A simple fluorescent probe for detecting mercury(II) ion in aqueous solution and on agar gels. J. Iran. Chem. Soc. **14**, 1207–1214 (2017). https://doi.org/10.1007/s13738-017-1071-7
43. Sun, Y., Wang, L., Zhou, J., Qin, D., Duan, H.: A new phenothiazine-based fluorescence sensor for imaging Hg^{2+} in living cells, 34:e5945. Appl. Organomet. Chem. (2020). https://doi.org/10.1002/aoc.5945
44. Yin, P., Niu, Q., Yang, Q., Lan, L., Li, T.: A new "naked-eye" colorimetric and ratiometric fluorescent sensor for imaging Hg^{2+} in living cells. Tetrahedron **75**, 130687 (2019). https://doi.org/10.1016/j.tet.2019.130687
45. Lee, J.J., Kim, Y.S., Nam, E., Lee, S.Y., Lim, M.H., Him, C.: A PET-based fluorometric chemosensor for the determination of mercury(ii) and pH, and hydrolysis reaction-based colorimetric detection of hydrogen sulfide. Dalton Trans. **45**, 5700–5712 (2016). https://doi.org/10.1039/C6DT00147E
46. Wang, J.H., Liu, Y.M., Dong, Z.M., Chao, J.B., Wang, H., Wang, Y., Shuang, S.: New colorimetric and fluorometric chemosensor for selective Hg^{2+} sensing in a near-perfect aqueous solution and bio-imaging. J. Hazard. Mater. **382**, 121056 (2020). https://doi.org/10.1016/j.jhazmat.2019.121056
47. Maity, A., Sil, A., Nad, S., Patra, S.K.: A highly selective, sensitive and reusable BODIPY based 'OFF/ON' fluorescence chemosensor for the detection of Hg^{2+} ions. Sens. Actuators B **255**, 299–308 (2018). https://doi.org/10.1016/j.snb.2017.08.016
48. Mohan, B., Sharma, H.K.: Synthesis of calix[6]arene and transduction of its fur fural derivative as sensor for Hg(II) ions. Inorganica Chim. Acta. **486**, 63–68 (2019). https://doi.org/10.1016/j.ica.2018.10.022
49. Liu, D., Wang, Y., Wang, R., Wang, B., Chang, H., Chen, J., Yang, G., He, H.: Fluorescein-based fluorescent sensor with high selectivity for mercury and its imaging in living cells. Inorg. Chem. Commun. **89**, 46–50 (2018). https://doi.org/10.1016/j.inoche.2018.01.016
50. Ngororabanga, J.M.V., Moyo, C.B., Tshentu, Z.R.: A novel multidentate pyridyl ligand: a turn-on fluorescent chemosensor for Hg^{2+} and its potential application in real sample analysis. Spectrochim. Acta A. **242**, 118651 (2020). https://doi.org/10.1016/j.saa.2020.118651
51. Fern´andez-Alonso, S., Corrales, T., Pablos, J.L., Catalina, F.: A Switchable fluorescence solid sensor for Hg^{2+} detection in aqueous media based on a photo crosslinked membrane functionalized with (benzimidazolyl)methyl-piperazine derivative of 1,8-naphthalimide. Sens. Actuators B **270**, 256–262 (2018). https://doi.org/10.1016/j.snb.2018.05.030
52. Liu, D., Zhu, H., Shi, J., Deng, X., Zhang, T., Zhao, Y., Qi, P., Yang, G., He, H.: 1, 8-Naphthalimide-based fluorescent sensor with high selectivity and sensitivity for Hg^{2+} in aqueous solution and living cells. Anal. Methods. **11**, 3150–3154 (2019). https://doi.org/10.1039/C9AY00711C
53. Kraithong, S., Panchan, W., Charoenpanich, A., Sirirak, J., Sahasithiwat, S., Swanglap, P., Promarak, V., Thamyongkit, P., Wanichacheva, N.: A method to detect Hg^{2+} in vegetable via a "Turn–ON" Hg^{2+}–fluorescent sensor with a nanomolar sensitivity. J. Photochem. Photobiol. A **389**, 112224 (2020). https://doi.org/10.1016/j.jphotochem.2019.112224
54. Bhaskar, R., Sarveswari, S.: Thiocarbohydrazide based Schiff base as a selective colorimetric and fluorescent chemosensor for Hg^{2+} with "Turn-Off" fluorescence responses. Chem. Select. **5**, 4040–4057 (2020). https://doi.org/10.1002/slct.202000652
55. Bag, S.S., De, S.: Pyrenylthioureayl alanine as a switch-on fluorescent sensor for Hg(II) ions. Anal. Chem. **3**, 11758–11764 (2018). https://doi.org/10.1002/slct.201802249
56. Saikia, D., Dutta, P., Sarma, N.S., Adhikary, N.C.: CdTe/ZnS core/shell quantum dot-based ultrasensitive PET sensor for selective detection of Hg (II) in aqueous media. Sens. Actuators B **230**, 149–156 (2016). https://doi.org/10.1016/j.snb.2016.02.035
57. Wu, L.L., Wang, Z., Zhao, S.N., Meng, X., Song, X.Z., Feng, J., Song, S.Y., Zhang, H.J.: A metal–organic framework/DNA hybrid system as a novel fluorescent biosensor for mercury(II) ion detection. Chem. Eur. J. **22**, 477–480 (2016). https://doi.org/10.1002/chem.201503335
58. Marieeswaran, M., Panneerselvam, P.: Fluorescent polyaniline nanoclips (PANCs): a highly sensitive and selective chemical sensor for the detection of Hg (II) ions in aqueous media. Anal Chem. **5**, 4481–4487 (2020). https://doi.org/10.1002/slct.202000545
59. Bhatti, A.A., Oguz, M., Yilmaz, M.: New water soluble p-sulphonatocalix[4]arene chemosensor appended with rhodamine for selective detection of Hg^{2+} ion. J. Mol. Structure. **1203**, 127436 (2020). https://doi.org/10.1016/j.molstruc.2019.127436
60. Horzum, N., Mete, D., Karakus, E., Ucuncu, M., Emrullahoglu, M., Demir, M.M.: Rhodamine-immobilised electrospun chitosan nanofibrous material as a fluorescence turn-on Hg^{2+} sensor. Chem. Select. **5**, 896–900 (2016). https://doi.org/10.1002/slct.201600027
61. He, W., Liu, R., Liao, Y., Ding, G., Li, J., Liu, W., Wu, L., Feng, H., Shi, Z., He, M.: A new 1,2,3-triazole and its rhodamine B

derivatives as a fluorescence probe for mercury ions. Anal. Biochem. **598**, 113690 (2020). https://doi.org/10.1016/j.ab.2020.113690
62. Kunthom, R., Piyanuch, P., Wanichacheva, N., Ervithayasuporn, V.: Cage-like silsesequioxanes bearing rhodamines as highly sensitive and selective fluorescence Hg^{2+} sensors. J. Photochem. Photobiol. A. **356**, 248–255 (2018). https://doi.org/10.1016/j.jphotochem.2017.12.033
63. Yang, Y., Shen, R., Wang, Y.-Z., Qiu, F.-Z., Feng, Y., Tang, X.-L., Bai, D., Zhang, G.-L., Liu, W.-S.: A selective turn-on fluorescent sensor for Hg (II) in living cells and tissues. Sens. Actuators B. 255:3479–3487 (2018). https://doi.org/10.1016/j.snb.2017.09.180
64. Wang, Q., Jina, L., Wang, W., Hu, T., Chen, C.: Rhodamine derivatives as selective "naked-eye" colorimetric and fluorescence off-on sensor for Hg^{2+} in aqueous solution and its applications in bioimaging. J. Lumin. **209**, 411–419 (2019). https://doi.org/10.1016/j.jlumin.2019.02.024
65. Xu, X., Zheng, B., Deng, H., Zhang, X., Shuai, Q.: Synthesis and sensing behavior of a new multichannel sensor based on thiazolyl ferrocene-rhodamine for Hg^{2+} detection. Microchem. J. **158**, 105257 (2020). https://doi.org/10.1016/j.microc.2020.105257
66. Petdum, A., Faichu, N., Sirirak, J., Khammultri, P., Promarak, V., Panchan, W., Sooksimuang, T., Charoenpanich, A., Wanichacheva, N.: [5]Helicene-rhodamine 6 G hybrid-based sensor for ultrasensitive Hg^{2+} detection and its biological applications. J. Photochem. Photobiol. A. **394**, 112473 (2020). https://doi.org/10.1016/j.jphotochem.2020.112473
67. Tsai, H.-J., Wan, C.-F., Su, Y., Wu, A.-T.: A selective colorimetric fluorescent chemosensor for Hg^{2+} in aqueous medium and in the solid state. J. Lumin. **194**, 279–283 (2018). https://doi.org/10.1016/j.jlumin.2017.10.023
68. Bai, C.-B., Qiao, R., Liao, J.-X., Xiong, W.-Z., Zhang, J., Chen, S.-S., Yang, S.: A highly selective and reversible fluorescence "OFF-ON-OFF" chemosensor for Hg^{2+} based on rhodamine-6G dyes derivative and its application as a molecular logic gate. Spectrochim. Acta A Mol. Biomol. Spectrosc. **202**, 252–259 (2018). https://doi.org/10.1016/j.saa.2018.05.050
69. Anandababu, A., Anandan, S., Ashokkumar, M.: A simple discriminating p-tert-butylcalix[4]arene thiospirolactam rhodamine b based colorimetric and fluorescence sensor for mercury ion and live cell imaging applications. Chem. Select. **3**, 4413–4420 (2018). https://doi.org/10.1002/slct.201800044
70. Hong, M., Chen, Y., Zhang, Y., Xu, D.: A novel rhodamine-based Hg^{2+} sensor with a simple structure and fine performance. Analyst. **144**, 7351–7358 (2019). https://doi.org/10.1039/C9AN01608B
71. Gao, T., Lee, K.M., Kim, S.H., Heo, J., Yang, S.I.: A Mercuric ion selective fluorescent sensor based on rhodamine B with an ethylene unit. Bull. Korean Chem. Soc. **38**, 292–295 (2017). https://doi.org/10.1002/bkcs.11078